ISSN 1288-1619

CNRS - Université Pierre et Marie Curie - Université Versailles-Saint-Quentin
CEA - ORSTOM - Ecole Normale Supérieure - Ecole Polytechnique

Institut Pierre Simon Laplace
des Sciences de l'Environnement Global

Notes du Pôle de Modélisation

The Trident Pacific model Part 2: The thermodynamical model and the role of long equatorial wave reflection during the TOPEX/POSEIDON period

Jean-Philippe Boulanger and Christophe Menkes

IPSL - Laboratoire d'Océanographie Dynamique et de Climatologie

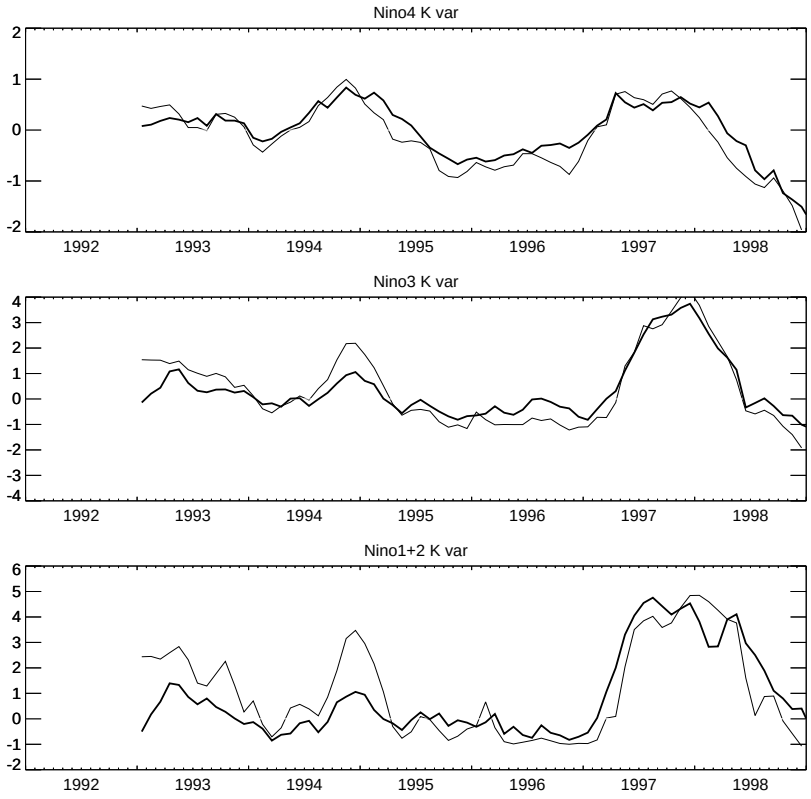

Janvier 2000 **Note n° 17**

I P S L

CNRS - Université Pierre et Marie Curie - Université Versailles-Saint-Quentin
CEA -CNES - ORSTOM - Ecole Normale Supérieure - Ecole Polytechnique

Institut Pierre Simon Laplace
des Sciences de l'Environnement Global

C E T P - LMD - LODYC - LPCM - LSCE - SA

Université Pierre-et-Marie-Curie
B 102 - T15-E5 - 4, Place Jussieu
75252 Paris Cedex 05 (France)
Tél : (33) 01 44 27 39 83
Fax : (33) 01 44 27 37 76

Université Versailles-Saint-Quentin
College Vauban, 47 Boulevard Vauban
78047 Guyancourt Cedex (France)
Tél : (33) 01 39 25 58 17
Fax : (33) 01 39 25 58 22

The present study is the continuation of a study initiated in Boulanger and Menkes (1999) and Boulanger (1999). It aims to give a quantitative description of the role played by long equatorial waves during the TOPEX/POSEIDON period and more specifically during the 1997-1998 ENSO period using a new Pacific Ocean model called Trident. In a companion paper, the Trident dynamical component was described and validated with observations. Briefly, the model has skills in simulating not only sea level but also surface zonal current variability in the equatorial wave guide. In the present paper, the model thermodynamics are described and validated. The Trident thermodynamics consist of one single equation for interannual sea surface temperature anomalies. Compared to other similar models, the introduction in the temperature equation of a term equivalent to a vertical mixing term improves significantly the temperature simulations in the eastern Pacific. Thus the model comparison to interannual sea level, zonal current and sea surface temperature anomalies is fairly good over the entire equatorial Pacific Ocean. The major active terms of the SST equation are found to be the zonal advection and vertical diffusion terms in the Niño3 box, and the zonal advection and vertical advection of anomalous termperatures in the Niño4 box. Thus the model is found to be sensitive not only to subsurface variability but also to zonal current advection especially near the dateline where data have suggested that it is a major process for sea surface temperature change. The role of long equatorial wave reflection observed in TOPEX/POSEIDON data is studied in Trident by either cancelling the eastern boundary or western boundary reflection. First, at the eastern boundary, although the reflected Rossby waves were found to act against the warming during the onset phase of the 1997-1998 El Niño through zonal advection, the major impact of these reflected Rossby waves was to reinforce the deepening of the thermocline in the eastern Pacific initated by the impinging Kelvin waves. Therefore, all things

Janvier 2000 , Note n° 17

Directeur de publication : Gérard Mégie, Directeur de l'IPSL
ISSN 1288-1619

being considered, the Rossby waves strongly contributed to the warming in 1997-1998 east of 120?W. Second, at the western boundary, Rossby wave reflection acted as suggested by the delayed action oscillator: the reflected Kelvin waves acted in shallowing the thermocline in the central and eastern Pacific where they weakened the warm or cold conditions observed in the Pacific Ocean. Specifically during the 1997-1998 event, they contributed to about a third of the upwelling Kelvin wave amplitude propagating in the central Pacific. The other two thirds of the amplitude were found to be actually wind-forced strongly suggesting that during that event easterly wind anomalies in the western Pacific played a significant role in the termination of the recent warm ENSO event and its switch to the La Niña period.

The Trident Pacific model

Part 2: The thermodynamical model and the role of long equatorial wave reflection during the TOPEX/POSEIDON period

Jean-Philippe Boulanger* and Christophe Menkes

*Laboratoire d'Océanographie Dynamique et de Climatologie
UMR CNRS/ORSTOM/UPMC
Université Pierre et Marie Curie
Tour 26/Etage 4/Case100
4 Place Jussieu
75252 Paris, Cedex 05
France
E-mail: jpb@lodyc.jussieu.fr

Submitted to *Climate Dynamics*
May 1999

Abstract

The present study is the continuation of a study initiated in Boulanger and Menkes (1999) and Boulanger (1999). It aims to give a quantitative description of the role played by long equatorial waves during the TOPEX/POSEIDON period and more specifically during the 1997-1998 ENSO period using a new Pacific Ocean model called Trident. In a companion paper, the Trident dynamical component was described and validated with observations. Briefly, the model has skills in simulating not only sea level but also surface zonal current variability in the equatorial wave guide. In the present paper, the model thermodynamics are described and validated. The Trident thermodynamics consist of one single equation for interannual sea surface temperature anomalies. Compared to other similar models, the introduction in the temperature equation of a term equivalent to a vertical mixing term improves significantly the temperature simulations in the eastern Pacific. Thus the model comparison to interannual sea level, zonal current and sea surface temperature anomalies is fairly good over the entire equatorial Pacific Ocean. The major active terms of the SST equation are found to be the zonal advection and vertical diffusion terms in the Niño3 box, and the zonal advection and vertical advection of anomalous termperatures in the Niño4 box. Thus the model is found to be sensitive not only to subsurface variability but also to zonal current advection especially near the dateline where data have suggested that it is a major process for sea surface temperature change. The role of long equatorial wave reflection observed in TOPEX/POSEIDON data is studied in Trident by either cancelling the eastern boundary or western boundary reflection. First, at the eastern boundary, although the reflected Rossby waves were found to act against the warming during the onset phase of the 1997-1998 El Niño through zonal advection, the major impact of these reflected Rossby waves was to reinforce the deepening of the thermocline in the eastern Pacific initated by

the impinging Kelvin waves. Therefore, all things being considered, the Rossby waves strongly contributed to the warming in 1997-1998 east of 120°W. Second, at the western boundary, Rossby wave reflection acted as suggested by the delayed action oscillator: the reflected Kelvin waves acted in shallowing the thermocline in the central and eastern Pacific where they weakened the warm or cold conditions observed in the Pacific Ocean. Specifically during the 1997-1998 event, they contributed to about a third of the upwelling Kelvin wave amplitude propagating in the central Pacific. The other two thirds of the amplitude were found to be actually wind-forced strongly suggesting that during that event easterly wind anomalies in the western Pacific played a significant role in the termination of the recent warm ENSO event and its switch to the La Niña period.

I. Introduction

The development of the observational networks over the tropical Pacific Ocean such as the Tropical Ocean Global Atmosphere – Tropical Atmosphere Ocean Array (Hayes et al., 1991; McPhaden, 1993), the thermal profile measurements by eXpendable BathyThermograph sondes, and various satellites (e.g. TOPEX/POSEIDON measuring sea-level, ERS measuring winds) provide for the first time the opportunity to observe, describe and understand the mechanisms involved in a strong El Niño/Southern Oscillation phenomenon such as the 1997-1998 event. Focusing on the oceanic processes potentially at work during ENSO, two theories (the delayed action oscillator, Schopf and Suarez, 1988; Battisti, 1988; Mantua and Battisti, 1994, and a revised theory, Picaut et al., 1997) are based on the dynamical and thermodynamical changes induced by long equatorial waves. In the former (the delayed action oscillator), reflection of Rossby waves at the western boundary is a crucial process in terminating a warm event through the thermocline displacements in the eastern Pacific. In the latter, reflection of Kelvin waves into Rossby waves at the eastern boundary plays a major role in the displacement of the eastern edge of the warm pool (highly correlated to the Niño3 index) through zonal advection. This displacement induces a feedback on the coupled system through the displacement of the atmospheric response mainly located west of the eastern edge of the warm pool (Picaut et al., 1996). While the former highlights the major role of vertical processes (thermocline displacement) in the central and east Pacific, the latter is based on the important role played by equatorial zonal surface currents via zonal advection.

Recently, Boulanger and Menkes (1999) described the observed variability in the equatorial Pacific during the TOPEX/POSEIDON period and more specifically during the 1997-1998 El Niño period. They offered the following qualitative description of the warm event. First, although

the westerly wind event in December 1996 slightly affected the equatorial conditions, the timing of the onset of the El Niño event seemed to be strongly related to the March 1997 westerly wind event located in the western Pacific. In relation to that atmospheric variability, the ocean responded by forcing a strong downwelling Kelvin wave which seemed to have contributed to the initiation of positive sea surface temperature anomalies in the far eastern Pacific and to the eastward displacement of the eastern edge of the warm-pool. Subsequently, westerly wind anomalies displaced to the central Pacific forcing large downwelling Kelvin waves propagating to the eastern Pacific and reflecting into Rossby waves. Although these reflected Rossby waves seemed to have contributed to a weak westward displacement of the 28°C, the positive sea surface temperature anomalies grew larger and the entire equatorial Pacific experienced temperatures higher than 28°C. At the western boundary, upwelling Rossby waves reflected into upwelling Kelvin waves. Strengthened by easterly wind anomalies observed in the western Pacific in early 1998, this upwelling Kelvin signal appeared to be responsible for the switch in the temperature anomalies from positive to negative in the central and eastern Pacific leading later to the development of a cold period.

The objective of the present study (Part 1 and Part 2) is to give a quantitative description of the processes involved during the 1997-1998 period by understanding the detailed mechanisms by which long equatorial waves contributed to the observed ENSO variability. Toward that end, an oceanic model of the Tropical Pacific Ocean, called Trident (Boulanger, 1999), has been developed to investigate the role of long equatorial wave reflection observed in TOPEX/POSEIDON data (Boulanger and Menkes, 1999). In a first part (Boulanger, 1999), the oceanic dynamics of the Trident model has been described and validated with various observations of the tropical Pacific Ocean. The model has three layers: two subsurface active

layers (i.e. two baroclinic modes) and a surface layer of constant depth. Fluxes of momentum and mass are only allowed between the surface layer and the first subsurface layer. The model comparison to TOPEX/POSEIDON sea level and TAO zonal current data showed the model skills in simulating both sea level and surface currents in the equatorial Pacific Ocean. Considering the model ability to simulate surface currents, we are confident in studying and discussing the respective roles of thermocline displacement and zonal advection in regulating sea surface temperature anomalies in the Trident model.

In this second part, the model thermodynamics is presented, and the role of long equatorial wave reflection at both the eastern and western boundaries are examined in the light of the two theories previously discussed. The model thermodynamics consist of one single equation for sea surface temperature interannual anomalies. In comparison with other similar models (Zebiak and Cane, 1987, Chen et al., 1995), an additional term is taken into account. This term has the form of a vertical mixing term and actually represents both the vertical diffusion of temperature in the surface layer and the effects of entrainment/detrainment not explicitly simulated as the surface mixed-layer has a constant depth. This new term in the temperature equation improves significantly the temperature variability in the eastern Pacific. In particular, the model is found to be sensitive not only to subsurface variability but also to zonal current advection especially near the dateline where it has been shown to be a crucial process for sea surface temperature changes (Picaut et al., 1996).

This paper is organized as follows. Section 2 presents the various data (ERS+TAO wind stress, sea surface temperature from the Climate Analysis Center and eXpendable Bathythermograph Temperature data set provided by Neville Smith). Section 3 describes the model thermodynamics. Section 4 discusses the model parameterizations. Section 5 compares the

model sea surface temperature anomalies to data during the 1992-1998 period. Section 6 describes the role of long equatorial wave reflection at the eastern and western boundaries on the dynamical and thermodynamical processes during the 1992-1998 period. Finally, Section 7 discusses the results and gives some conclusions.

II. Data

EXpendable BathyThermograph (XBT) data. The XBT data set is a three-dimensional interpolated data set kindly provided by Neville Smith (Smith, 1995). Data are monthly averaged and gridded onto a 2° longitude by 1° latitude horizontal grid and onto a vertical grid identical to the Levitus climatology (Levitus, 1982). The period covered extends from January 1980 to December 1998. For the sake of consistency with shorter data sets, climatology is computed over the period 1993-1996. Interannual anomalies are computed relative to this period. This data set was also used to compute dynamic height relative to 400dbar.

Sea surface temperature data. Sea surface temperature data, obtained from the Columbia University web site (**Erreur! Signet non défini.**, were compiled by the NOAA Climate Analysis Center. The period covered by the data is January 1970 - December 1998. Data originally on a 2° longitude by 2° latitude are interpolated onto the model grid (2° longitude by 0.5° latitude). For the sake of consistency with shorter data sets, climatology is computed over the period 1993-1996. Interannual anomalies are computed relative to this period.

III. The model thermodynamics

Thermodynamics equation. The model basin geometry and the model grid are displayed in Boulanger (1999). The thermodynamics equation is computed on a C-grid with a resolution identical to the oceanic model resolution (2° in longitude, 0.5° in latitude). The temperature grid extends from 131°E to 81°W in longitude and from 20°S to 20°N in latitude.

The computation of sea surface temperature anomalies is performed using a single equation as in Zebiak and Cane (1987) and Chen et al. (1995). A difference to these two studies is an additional term added to the equation representing a temperature vertical mixing at the base of the model constant mixed-layer. It will be shown to significantly improve the model simulation of SSTA in the eastern Pacific

The thermodynamical equation has the following form (where barred quantities represent seasonal fields and unbarred quantities interannual anomalies):

$$\partial_t T = -\partial_x \left[\left(\overline{T} + T \right) u \right] + \left(\overline{T} + T \right) \partial_x u \quad (1)$$

$$- \partial_x \left[\overline{u} T \right] + T \partial_x \overline{u} \quad (2)$$

$$- \partial_y \left[\left(\overline{T} + T \right) v \right] + \left(\overline{T} + T \right) \partial_y v \quad (3)$$

$$- \partial_y \left[\overline{v} T \right] + T \partial_y \overline{v} \quad (4)$$

$$- \left[M(\overline{w} + w) - M(\overline{w}) \right] \partial_z \overline{T} \quad (5)$$

$$- M(\overline{w} + w) \partial_z T \quad (6)$$

$$+ K_T \partial_z T \quad (7)$$

$$+ A_H \Delta_H T \quad (8)$$

$$- r_T T \quad (9)$$

where M(x) is a function equals to x for x positive and 0 otherwise.

The first four terms of the thermodynamics equation respectively represent the zonal advection of temperature by the anomalous currents, the zonal advection of the anomalous temperature by seasonal currents, the meridional advection of temperature by the anomalous

currents, and the meridional advection of the temperature by seasonal currents. Their forms are numerically accurate as the temperature grid is a C-grid. When presenting the advection terms as above, terms (2) and (4) cannot create any temperature anomalies without these being already present, while the terms (1) and (3) can create temperature anomalies as soon as anomalous currents are present in the basin. Thus, the latter terms can be seen as initiators of temperature anomalies, while the former terms are reacting to these anomalies. The fifth and sixth terms respectively represent the anomalous vertical advection of seasonal temperature and the vertical advection of anomalous temperature. Term (7) is new and equivalent of a vertical mixing term with the value of K_T chosen to 3.10^{-5} in the eastern Pacific. It will be discussed later. Term (8) is a horizontal diffusion term with a coefficient identical to the one used in the shear layer equation (A_H=2000$m^2.s^{-1}$ at the equator; see Boulanger, 1999). Finally term (9) is a friction term applied to the temperature anomalies and is a crude representation of interannual heat fluxes (r_T=$(125days)^{-1}$). The climatology used here is the one described in section IV of Boulanger (1999).

Subsurface temperature data. In order to compute terms (5), (6), and (7) we need to define the following terms: the seasonal temperature vertical gradient $\partial_z \overline{T}$ and the anomalous temperature vertical gradient $\partial_z T = (T - T_{sub}) / H_{mix}$ where H_{mix} is the model mixed-layer and T_{sub} represents subsurface temperature anomalies at the base of the mixed-layer. To compute a subsurface temperature data set, interpolated XBT fields provided by Neville Smith (Smith, 1995) are first used to estimate a mixed-layer depth defined as the depth where the temperature is lower than the surface temperature by 0.5°C (Hayes et al., 1991; Wang and McPhaden, 1999a,b). Figure 1 displays the mean mixed-layer field as well as the variability of the seasonal cycle (computed over 1993-1996) and interannual variability (over the period 1980-1998). No significant pattern or amplitude differences would be found if the mean and seasonal cycle were

computed over the 1980-1998 period. The general features are in good agreement with the usual description of the tropical Pacific ocean although the lack of salinity data may alter the computation of the mixed-layer depth especially in the western Pacific. A shallower mixed-layer is found in the eastern Pacific and in the western Pacific while a deeper one is observed in the central Pacific. The seasonal cycle variability is rather weak (around 10m at maximum) in the equatorial band, while the interannual variability is twice as large especially near the dateline where interannual wind anomalies are located.

Considering that the model mixed-layer has a constant depth of 50m, we construct a subsurface temperature such that the temperature vertical gradient computed over 50m would be equal to the vertical gradient computed from data. It is then straightforward to show that the equivalent subsurface temperature at 50m is: $T_{sub} = SST - 0.5(50/h_{ML})$ where h_{ML} is the mixed-layer depth computed from XBT data. A climatology relative to the 1993-1996 period is then computed as well as interannual anomalies. Figure 2 displays the mean susburface temperature field as well as seasonal and interannual variability. The mean field is very much similar to the sea surface temperature mean field with a cold tongue extending from the eastern Pacific along the coast to the central Pacific along the equator. Larger temperatures are found in the western Pacific and north of the equator mainly along the North Equatorial Counter Current. Most of the seasonal variability is located in the eastern Pacific along the South American coasts reaching up to 2.25°C. Interannual anomalies have a pattern of large variability strongly related to the structure of the cold tongue i.e. of the coastal and equatorial upwelling.

The subsurface temperature data set is first used to compute a seasonal vertical gradient of temperature using the CAC seasonal sea surface temperature data (Figure 3). During spring when the Trades are weaker and the eastern Pacific experiences a seasonal warming, the vertical

gradient almost reaches 5°C/100m and extends with large values far along the equator. All other seasons appear weaker except around 10°N along the coast in fall. Besides large amplitudes are observed along the South American coasts mainly in boreal winter and spring. The seasonal vertical gradient of temperature is used in the following to compute the term (5) of the thermodynamics equation.

With the subsurface temperature interannual anomalies at hand, a parameterization has been developed to relate these anomalies to sea level anomalies following an approach similar to Zebiak and Cane (1987). The parameterization chosen here has the following form:

$$T_{sub} = T_1 \tanh(h/h_1) \quad \text{if} \quad h < 0$$
$$T_{sub} = T_2 \tanh(h/h_2) \quad \text{if} \quad h > 0$$

Here different tests had been made computing the four unknown parameters using as sea level anomalies either dynamic height anomalies computed from XBT data over the 1980-1998 period or over the 1993-1998 period or TOPEX/POSEIDON sea level anomalies over the 1993-1998 period (all anomalies are computed relative to the 93-96 mean seasonal cycle). First it was found (not shown here) that when the XBT data set was used over the entire period, spatial patterns of the four parameters were rather noisy certainly due to insufficient data coverage along the equator prior to the development of the TOGA-TAO Array. Then it appeared that the variability of T/P data especially near the american coasts was larger than in dynamic height data. As a consequence and despite the short period under study (6 years), the quality of the T/P data led to the choice of computing the four parameters from T/P sea level anomalies over the period 1993-1998 period. There is no doubt however that longer time series will certainly help in improving the subsurface parameterization. The four coefficients are plotted in Figure 4. The coefficients T_1 and T_2 represent the maximum amplitudes that the subsurface temperature anomalies can reach.

The coefficients h_1 and h_2 represent a sea level amplitude. The smaller they are, the smaller a sea level anomaly needs to be for a subsurface temperature anomaly to reach its maximum (T_1 or T_2). Finally Figure 4 also displays the subsurface temperature anomalies related to a 10cm sea level anomaly over the entire basin.

The patterns displayed when the sea level anomalies are negative or positive are very different. When h<0, the maximum subsurface temperature anomalies (Fig. 4a) are found near 140°W-120°W in a region where the mean thermocline starts deepening. In that region, the upwelling of the thermocline affects more strongly the subsurface anomalies than further east where the thermocline is already close to the surface. However it also appears that the regions of large subsurface temperature amplitudes i.e. in the 140°W-120°W region along the equator are not as sensitive to small negative sea level anomalies than regions closer to the eastern boundary (Fig. 4b). As a conclusion (Fig. 4c), it appears that for a 10cm sea level anomaly, the region with the largest response is located near 110°W. When h>0, the region closer to the eastern boundary (east of 120°W) displays the largest subsurface temperature amplitudes (Fig. 4d) with a maximum close to 100°W. However as h_2 is smaller close to the eastern boundary (Fig. 4e), the region of larger response to a 10cm sea level anomaly (Fig. 4f) is rather located near the eastern boundary along the coast extending westward along the equator.

To evaluate the skill of this parameterization, the parameterized subsurface temperature anomalies are compared to the original data set (Fig. 5). It appears that the two fields are well correlated especially east of 160°E and west of 170°W in the equatorial wave guide. However the correlation values are the smallest near the dateline where it has been found that the sea surface temperature anomalies are more likely to be determined by zonal advection. It is thus likely that in this region of usually deep thermoclines the temperature variability at the base of the mixed-

layer would be more affected by other processes than vertical ones. In the western Pacific, the slowly increasing correlations may be due to an interaction between long equatorial waves and the mixed-layer depth as can be seen in OGCMs (J. Vialard, personal communication). On average the rms difference is on the order of 0.3°C with larger values close to the eastern boundary. As a conclusion, the subsurface parameterization fairly well represents the subsurface field especially along the equator and near the eastern boundary where the anomalies are the largest (Fig. 5).

IV. Validation of the thermodynamics equation

To evaluate the model skill in simulating SSTA during the 1993-1998 period, three experiments have been performed. The first simulation (SST0) is run without the vertical mixing term (term (7)) i.e. with physics similar to the one of the Zebiak and Cane (1987) or the Chen et al. (1995) models although we use our own parameterizations. When comparing the Niño indices to the observed ones (Fig. 6, Table 1), the simulation compares very well to the Niño3 and Niño4 indices although it misses the coastal warming in 1997-1998, and part of the positive amplitude in 1997. However the Niño indices average large areas and actually a model evaluation using the Niño indices only can hide local discrepancies between observed and simulated SSTA as seen in Figure 7 east of 110°W . Indeed, the model simulates large SSTA in the region of large upwelling velocity, but neither simulates the coastal variability nor the northward and southward extension of the anomalies in the eastern Pacific. Not only correlations to observations drop in that region, but also the simulated variability north of the equator in the eastern Pacific is very weak as compared to observations. South of the equator, the upwelling intensity is not strong enough to

explain the amplitude of the variability. In particular in the Northern Hemisphere where the model simulates a strong downwelling, the model thermodynamics is not sensitive to any subsurface temperature anomalies as the term (6) is mostly equal to zero. Therefore this simplified model for the SST equation is unable to create strong positive SSTA north of the equator in the eastern Pacific during an El Niño (contrary to what is observed in data).

To improve the model simulation of SSTA variability, focus has been brought in adding physics to the SST equation. The improvement of SST simulations in the east Pacific has been achieved by introducing the term (7) in the SST equation. This term is actually a crude representation of two major mechanisms in the upper-ocean surface layer: vertical mixing and entrainement/detrainement of the mixed-layer. To optimize the value of K_T , considering that SSTA are most sensitive to sea level anomalies in the eastern Pacific, comparisons between observed and simulated SSTA were first performed for different values of K_T in the area including the two regions 5°N-5°S/130°W-90°W and 10°N-10°S/90°W-80°W. Results (not shown here) led to the choice of a value equal to 3.10^{-5}m.s^{-1}.

Actually in the eastern Pacific no significant differences would be found if using a larger value. Such a value for K_T is larger than the model mean equatorial upwelling in the central Pacific (around 2m/days). As a consequence, if K_T was kept constant over the entire basin, the model variability of SSTA would be strongly controlled by sea level anomalies over the entire Pacific. Such a result would actually be in contradiction with observations (Fig. 8) and to the fact that zonal advection plays a crucial role in the central Pacific (Picaut et al., 1996). As an illustration, if the model is run with a constant value for K_T (run SST1), the comparison with the Niño4 index is much worse (Fig. 9, Table 1). Besides, the model shows a good correlation in the Niño1+2 box and a better representation of the 1997-1998 warming along the coast. However it

appears to overestimate the anomalies in 1994-1995. As will be shown later, this overestimation is related to an overestimation of the model sea level anomalies forced by the ERS+TAO wind data at that period.

As a consequence to the comparison displayed in Figure 9, the vertical mixing coefficient is defined to be spatially variable. Considering that SSTA and SLA data show a larger correlation (Fig. 8) in the western and eastern Pacific than in the central Pacific, the dependence is built on the spatial variability of the mean mixed-layer depth (Fig. 1a) rather than of the mean thermocline depth. The computation of the spatial structure of K_T is a decreasing function of the mean mixed-layer depth:

$$K_T(x,y) = 3.10^{-5} \quad \text{if} \quad H_{ML}(x,y) \le 40\,\text{m}$$
$$K_T(x,y) = \max(3.10^{-5} x 10^{(-(H_{ML}(x,y)-40)/5)}, 2.10^{-9}) \quad \text{if} \quad H_{ML}(x,y) \ge 40\text{m}$$

where 2.10^{-9} represents the molecular diffusivity for the temperature (10^{-7}) divided by the model mixed-layer.

With this new formulation, the model-data comparison (run SSTR) is improved in terms of the Niño indices (Fig. 10; Table 1) as well as spatially over the basin (Fig. 11). Therefore the major effect of including the term (7), even if it is a crude representation of vertical mixing, is to improve the simulation of sea surface temperature anomalies along the eastern boundary coasts and along the equator east of 140°W. However due to the wind forcing, to the model dynamics, to data onto which the parametrization is developped, to the simplicity of the model parametrizations (including the formulation of heat fluxes), the rms difference between the model and data is still larger than 1°C at the eastern boundary.

V. Interannual variability during the 1993-1998 period

In a recent study, Boulanger and Menkes (1999) described the variability of interannual sea level, zonal current and sea surface temperature anomalies during the October 92 - May 98 period. The data period now under study is extended to December 98 (Figure 12a-c) and compared to the simulated fields (Fig. 13a-c). There is a good agreement between the observed and simulated interannual anomalies as the model is able to reproduce both the phase and the amplitude of SLA, ZCA and SSTA. It is important to note that observed ZCA are geostrophic currents derived from TOPEX/POSEIDON sea level anomalies which do not include the locally wind-forced shear component. This explains the large differences between model and data especially in March 1997 and June-July 1997 when strong westerly wind anomalies are located in the western and central Pacific. Overall, Trident forced by ERS+TAO winds performs well in simulating the interannual east-west sea level seasaw. However it appears that the sea level positive amplitude is slightly larger than observations in the eastern Pacific in 1994-1995 while it is weaker during the 1997-1998 El Niño. As a consequence in this region where the sea surface temperature anomalies strongly respond to sea level anomalies, the simulated temperature positive anomalies are larger in 1994-1995 and slightly weaker during the warm ENSO event. However it is important to note that, during the entire period, the model fairly well simulates the zonal current anomalies in term of amplitude and variability. Hence during the strong ENSO event, the model reproduces the large eastward current anomalies which contributed in displacing the warm-pool eastward. Therefore the Trident model forced by ERS+TAO winds has a good skill in simulating the observed interannual anomalies in the equatorial Pacific during the T/P period and more specifically during the 1997-1998 El Niño event. Before examining how long equatorial wave reflection at both the eastern and western boundaries contributed to the onset,

development and termination of the last ENSO, the variability of the various terms of the SSTA equation are now discussed.

In the Niño3 region (Fig. 14), the major terms involved in the SSTA evolution are the zonal advection terms, the vertical diffusion term and the damping although some contribution can happen episodically from the other terms. Mainly, it is worth noting that the zonal advection term by anomalous currents and the vertical diffusion term are in phase during the warming in late 1994-early 1995 and during the onset and development of warm conditions in 1997 both leading to create positive SSTA. Zonal advection in the Niño3 region did favor warm conditions during the entire 1997-1998 El Niño period. This result suggests that despite the potential role played by the Rossby waves reflected at the eastern boundary in counteracting the warming (Picaut et al., 1997; Boulanger and Menkes, 1999), Rossby wave zonal advection was not able to explain the weakening of the warm conditions, neither the onset of cold conditions in the central-eastern Pacific. Indeed, in late 1997-early 1998 when observed SSTs were almost homogeneous over the basin, the zonal gradient of temperature was very weak and the zonal advection could not play any major role then. It is the vertical diffusion term mainly related to sea level anomalies which shows a huge drop in its contribution to SSTA variability from 1997 to 1998 when the warm conditions weakened and reversed to cold anomalies suggesting that it was this term which mostly contributed to the reversal of the anomalies in the east.

In the Niño4 region (Fig. 15), the vertical diffusion term does not play any role. However both the zonal advection terms and the vertical advection of anomalous temperature play a significant role in the SSTA evolution. Focusing on the last ENSO events, two peaks in term (1) are observed in relation to the two westerly wind events observed respectively in December 1996

and March 1997 in the western Pacific. However the contribution of term (1) weakens quickly in 1997 when warm SSTs extend over the entire basin reducing significantly the zonal gradient. Then as the zonal gradient of anomalous temperatures grew larger (and positive), zonal advection by seasonal currents (mainly westward) largely contributed to a warm tendency in 1997 and early 1998. This trend was partially counteracted by the vertical advection of anomalous temperatures and the damping term.

VI. Role of long equatorial wave reflection

Eastern boundary reflection. Boulanger and Menkes (1999) investigated long equatorial wave reflection at the eastern boundary. They showed that they occured during the entire T/P period (1992-1998) with a 75% reflection efficiency. They also argued that the data suggested a decrease in the reflected Rossby signal from the eastern boundary. In order to investigate the role of these reflected Rossby waves, the model was run with no eastern boundary reflection, and the difference with the control run was computed in terms of SLA, ZCA and SSTA (Fig. 16a-c). Large differences in sea level anomalies are observed near the eastern boundaries from which the reflected signal decreases rapidly. Thus a large impact of removing the eastern boundary reflection is to weaken the sea level anomalies in the eastern Pacific as suggested by data (Boulanger and Menkes, 1999). However the reflected Rossby wave is interesting in that its sea level and surface current anomalies tend to act in opposite ways. While the thermocline anomalies reinforce the ones initated by impinging Kelvin waves, therefore strengthening the local anomalies through vertical processes, the zonal current anomalies cancel the Kelvin wave current anomalies and act in pushing the waters westward during an El Niño event, eastward during a La Niña event. Focusing on the zonal advection process, Picaut et al. (1997) described

reflected Rossby waves as a potential contributor to the termination of warm events. Indeed, during the 1997-1998 event, large westward surface currents due to reflected Rossby waves extend far into the eastern and central Pacific (Fig. 16b). However, the major impact on SSTA when removing reflection at the eastern boundary is to reduce the amplitude of the anomalies in the eastern Pacific. It clearly appears on Figures 16a that reflected Rossby waves strongly acted during the warm event in strengthening the warm anomalies up to 160°W in Spring 1998. It is only near 140°W in late 1997 and near the dateline in Spring 1998 that reflected Rossby waves contributed in weakly cooling the ocean while their sea level anomalies were downwelling throughout the basin. Therefore these weak coolings clearly indicate that reflected Rossby waves acted through zonal advection in slightly weakening the warming during these two periods. However these anomalies are rather weak compared to the large warming east of 110°W. To better evaluate the actual role of reflected Rossby waves, differences of the SSTA terms in the Niño3 region between the control run and the one with no eastern boundary reflection are computed. It appears (Fig. 17) as advocated by Picaut et al. (1997) and as suggested by observations (Boulanger and Menkes, 1999) that the reflected Rossby waves played a role during the 1997 year in cooling the warm conditions through zonal advection.

Western boundary reflection. Boulanger and Menkes (1999) found reflection to occur during the entire period, although the negative Kelvin wave amplitude in late 1997-early 1998 could not be explained by the reflection only. To quantify the actual Kelvin wave amplitude coming from the western boundary reflection, the model is run with no western boundary reflection. The difference with the control run is then computed. In terms of sea level anomalies (Fig. 18), the entire basin is affected in agreement with the basic principles of the delayed action oscillator mechanism although the largest differences in the model are in the western Pacific.

Focusing on the 1997-1998 period, the western boundary reflection explains up to -8cm at 150°E when the simulated negative signal is lower than -20cm. Therefore the reflection explains about a third of the control run signal, and the anomalous easterly winds explain about two thirds of the upwelling Kelvin signal propagating eastward. Whether the western boundary reflection is negligeable compared to the effect of wind anomalies in the reversal of the sea surface temperature anomalies from warm to cold will require examining a coupled model simulation. In terms of surface zonal currents, the reflected Kelvin waves do not contribute significantly to the equatorial surface currents for two reasons. First, as previously said, a large part of the Kelvin wave is wind-forced in the western Pacific. Second, the Rossby waves which largely contribute to the equatorial zonal currents are not affected significantly by the loss of Kelvin wave amplitude impinging at the eastern boundary. The impact on sea surface temperature anomalies is therefore straightforward: reflected Kelvin waves tend to cool the ocean during warm conditions, and to warm the ocean during cold conditions. This is the basic principle of the delayed action oscillator mechanism. The difference of the SSTA terms (Fig. 19) between the two simulations confirms these results as the major difference is found in term (7) directly related to sea level displacement.

VII. Discussion and conclusions

In a recent paper, Boulanger and Menkes (1999) investigated long equatorial wave reflection during the 1992-1998 period observed by TOPEX/POSEIDON. They found evidence that the western boundary acted as a perfect reflector for long first-mode Rossby waves and that the eastern boundary was reflecting Kelvin waves into Rossby waves with a reflection efficiency of 75% of that of an infinite meridional wall. With the existence of boundary reflection at hand,

they examined qualitatively the delayed action oscillator mechanism and the revised theory proposed by Picaut et al. (1997). Their study led them to the conclusion that although both theories needed to be considered simultaneously to understand the oceanic variability during the 1997-1998 El Niño event, western boundary reflection and wind-forcing in the western Pacific were more likely to explain the decay phase of the warm event. The aim of the present work is to bring a more quantitative estimate of the role of long equatorial waves and their reflection during the strong 1997-1998 warm ENSO.

A preliminary step has been to develop a model of the equatorial Pacific basin, which could be used as a reliable tool to understand the role of long equatorial waves. This simple ocean model, named Trident, is composed of a dynamical and a thermodynamical component. Briefly, the ocean dynamics (Boulanger, 1999) shows a good skill in representing the sea level variability (T/P sea level data) and equatorial surface currents (TAO surface currents at 10m) giving confidence in using it to assess the respective role of thermocline displacement and zonal advection on SSTA variability.

Similarly to other simple models (Zebiak and Cane, 1987; Battisti, 1988; Chen et al., 1995), the sea surface temperature interannual anomalies are computed using one single equation and assuming a constant mixed-layer of 50m. When computing SSTA with the same physics as these models, it is found that the Niño3 and Niño4 indices are well represented. However, this good comparison hides discrepancies mainly located in the eastern equatorial Pacific where the mean downwelling vertical current does not allow the model to simulate large temperature anomalies as observed. Therefore a new term, which is presented as a vertical mixing term, has been added to the SST equation. It has been shown to greatly improve the simulation of SSTA in the east Pacific. As in the central and western Pacific other processes such as zonal advection may play a

significant role in the interannual variability of SSTA, the vertical mixing coefficient is defined to be a spatially variable function of the mean mixed-layer depth computed from XBT data. This new parameterization helped in improving the simulation over the basin.

The model interannual anomalies in sea level, zonal currents and sea surface temperature at the equator reproduce fairly well observations (T/P sea level and derived geostrophic current anomalies, and CAC sea surface temperature anomalies). The study of the various terms of the SST equation shows that the major active contributions to SST changes are due to the zonal advection and vertical diffusion terms in the Niño3 box, and to the zonal advection and vertical advection of anomalous temperature in the Niño4 box. Moreover, despite the potential role of reflected Rossby waves in weakening the warm anomalies in 1997-1998 period, the zonal advection of interannual SSTA was never negative during the entire warm event and it became negligible once warm temperatures became almost homogeneous over the entire basin.

These previous comparisons to observations give confidence in using the model to study the role of reflected long equatorial waves during the TOPEX/POSEIDON period. Thus the model was first run with no eastern boundary reflection. It was shown that during the El Niño event, the Rossby waves may have played two opposite roles. On one hand, they contributed significantly to the downwelling sea level anomalies in the eastern Pacific i.e. it potentially increased the warming initated by the Kelvin waves. On the other hand, they had large westward currents which potentially advected the warm waters back to the central and western Pacific. Although very weak cooling events due to zonal advection by the reflected Rossby waves are observed near 130°W in late 1997 and near the dateline in Spring 1998, the major impact of reflected Rossby waves is found in the eastern Pacific (east of 140°W) where they strengthened the warm anomalies by deepening further the thermocline.

Then the model was run with no reflection at the western boundary. The major impact is in agreement with the basic principle of the delayed action oscillator mechanism as the effect of reflected Kelvin waves is mainly through the thermocline displacement and weakly through zonal current anomalies. During the warm 1997-1998 ENSO event, the reflected upwelling Kelvin waves acted in weakening the downwelling signals wind-forced in the central Pacific. However, the reflection at the end of the warm period only explains a third of the upwelling Kelvin signal in the western Pacific observed to propagate eastward. Therefore about two thirds of the Kelvin wave amplitude propagating eastward was actually wind forced highlighting the important role played by the wind-forcing in the western Pacific in the termination of the 1997-1998 El Niño, and possibly in the reversal to cold La Niña conditions.

Acknowledgements

The research described in this paper was initiated while Jean-Philippe Boulanger was at the Jet Propulsion Laboratory, California Institute of Technology, under contract with National Aeronautics and Space Administration. It was completed while Jean-Philippe Boulanger was working for Centre National de la Recherche Scientifique at Laboratoire d'Océanographie Dynamique et de Climatologie (LODYC, Jussieu, Paris). The authors thank the Center for Space Research from the University of Texas for providing the processed and gridded TOPEX/POSEIDON data (http://www.csr.utexas.edu/sst/gsdata.html), the Center ERS d'Archivage et de Traitement located in the Institut Francais de Recherche pour l'Exploitation de la Mer for providing the processed and gridded ERS-1 and ERS-2 zonal wind stress data (http://www.ifremer.fr/cersat/ARFTP/arftp.html), PMEL for providing TAO data, and Neville Smith who kindly made available his subsurface temperature analysis based on XBT data. Jean-Philippe Boulanger also thanks Lee-Lueng Fu for his constant support, Claire Perigaud for her fruitful comments, as well as all the people from the Ocean Science Element at JPL who helped me or with whom I had discussions during my 2-year stay there. The authors also thank Pascale Delecluse, Gurvan Madec, Gilles Reverdin, Jérôme Sirven, Jérôme Vialard and many people from LODYC who contributed to the evolution and design of the Trident model.

REFERENCES

Battisti D. S., Dynamics and thermodynamics of a warming event in a coupled tropical atmosphere-ocean model, *J. Atmos. Sc.*, **45**, 2889-2819, 1988.

Bentamy, A., Y. Quilfen, F. Gohin, N. Grima, M. Lenaour, and J. Servain, Determination and validation of average wind fields from ERS-1 scatterometer measurements, *The Global Atmopshere and Ocean System*, **4**, 1-29, 1996.

Boulanger, J.-P., The Trident Pacific model. Part 1: the oceanic dynamical model during the TOPEX/POSEIDON period, *Clim. Dyn*. submitted.

Boulanger, J.-P, and L.-L. Fu, Evidence of boundary reflection of Kelvin wave and first-mode Rossby waves from TOPEX/POSEIDON sea level data, *J. Geophys. Res.*, **101**, 16361-16371, 1996.

Boulanger, J.-P, and C. Menkes, Long equatorial wave reflection in the Pacific Ocean from TOPEX/POSEIDON during the 1992-1998 period, *Clim. Dyn.*, 1999, in press.

Boulanger, J.-P, and C. Menkes, Propagation and reflection of long equatorial waves in the Pacific ocean during the 1992-1993 El Niño, *J. Geophys. Res.*, **100**, 25041-25059, 1995.

Chen, Y.-Q., D. S. Battisti, and E. S. Sarachik, A new ocean model for studying the tropical oceanic aspects of ENSO, *J. Phys. Oceanogr*., **25**, 2065-2089, 1995.

Delcroix, T., J.-P. Boulanger, F. Masia, and C. Menkes, GEOSAT-derived sea level and surface-current anomalies in the equatorial Pacific, during the 1986-1989 El Niño and La Niña, *J. Geophys. Res*., **99**, 25093-25107, 1994.

Halpern, D., Observations of annual and El Niño thermal and flow variations at 0°, 110°W and 0°, 95°W during 1980-1985, *J. Geophys. Res.*, **92**, 7289-7312, 1987.

Hayes, S. P., L. J. Mangum, J. Picaut, A. Sumi, and K. Takeuchi: TOGA-TAO: A moored array for real-time measurements in the tropical Pacific ocean, *Bull. Am. Met. Soc*., **72**, 3,339-347, 1991.

Levitus, S., Climatological Atlas of the World Ocean. NOAA Professional Paper 13, U.S. Government Printing Office, 183pp., 1982.

Mantua, N. J. and D. S. Battisti, Evidence for the delayed oscillator mechanism for ENSO: The "observed" oceanic Kelvin mode in the far western Pacific, *J. Phys. Oceanogr*., **24**, 691-699, 1994.

McPhaden M. J., TOGA-TAO and the 1991-93 El Niño-Southern Oscillation event, *Oceanography,* **6**, 36-44, 1993.

Menkes, C., J.-P. Boulanger, A.J. Busalacchi, J. Vialard, P. Delecluse, M.J. McPhaden, E. Hackert, and N. Grima, Impact of TAO vs. ERS wind stresses onto simulations of the tropical Pacific Ocean during the 1993-1998 period by the OPA OGCM, *Climatic Impact of Scale Interactions for the Tropical Ocean-Atmosphere System*, pp. 46-48, Euroclivar Workshop Report, Eucliv 13, December 1998.

Picaut, J., F. Masia, and Y. duPenhoat, An advective-reflective conceptual model for the oscillatory nature of the ENSO, *Science*, **277**, 663-666, 1997.

Picaut, J., M. Ioualalen, C. Menkes, T. Delcroix, and M. J. McPhaden, Mechanism of the zonal displacements of the Pacific warm pool: implications for ENSO, *Science*, **274**, 1486-1489, 1996.

Picaut, J., and T. Delcroix, Equatorial wave sequence associated with warm pool displacements during the 1986-1989 El Niño-La Niña, *J. Geophys. Res*., **100**, 18393-18408, 1995.

Schopf, P. S., and M. J. Suarez, Vacillations in a coupled ocean-atmosphere model, *J. Atmos. Sci.*, **45,** 549-566, 1988.

Smith, N. R., An improved system for tropical ocean subsurface temperature analyses, *J. Atmos. Oceanic Technol.*, **12**, 850-870, 1995.

Wang, W, and M. J. McPhaden, The surface layer heat balance in the equatorial Pacific ocean, Part I: Mean seasonal cycle, *J. Phys. Oceanogr*., in press.

Wang, W, and M. J. McPhaden, The surface layer heat balance in the equatorial Pacific ocean, Part II: Interannual variability, *J. Phys. Oceanogr*., accepted.

Zebiak, S. E., and M. A. Cane, A model El Niño/Soutrhern Oscillation, *Mon. Wea. Rev*., **115**, 2262-2278, 1987.

FIGURE CAPTIONS

Figure 1: (a) Mean mixed-layer depth computed from XBT data over the period 1993-1996 (contours are every 10m; values higher than 50m are shaded). (b) Standard deviation of the mixed-layer depth seasonal cycle computed over the period 1993-1996 (contours are every 2m; values higher than 10m are shaded). (c)) Standard deviation of the mixed-layer depth interannual variability computed over the period 1980-1998 (contours are every 2m; values higher than 10m are shaded).

Figure 2: (a) Mean subsurface temperature computed from XBT data over the period 1993-1996 (contours are every 1°C; values higher than 25°C are shaded). (b) Standard deviation of the subsurface temperature seasonal cycle computed over the period 1993-1996 (contours are every 0.25°C; values higher than 1°C are shaded). (c)) Standard deviation of the subsurface temperature interannual variability computed over the period 1980-1998 (contours are every 0.25°C; values higher than 1°C are shaded).

Figure 3: Mean seasonal vertical gradient of temperature computed for the season (a) December-January-February; (b) March-April-May; (c) June-July-August; and (d) September-October-November (contours are every 0.5°C/100m; values higher than 1°C/50m are shaded).

Figure 4: Spatial maps of the coefficients defining the subsurface temperature parameterization. Contour intervals for the coefficients T_1 and T_2 are every 1°C. Contour intervals for the coefficients h_1 and h_2 are every 10cm. Contour intervals for the values $T_1\tanh(0.1/h_1)$ and $T_2\tanh(0.1/h_2)$are every 0.5°C.

Figure 5: (a) Map of correlation between XBT and parameterized subsurface temperature anomalies for January 1993-December 1998 (contour intervals are every 0.1); (b) Standard deviation of the XBT subsurface temperature anomalies (contour intervals are every 0.25); (c) Standard deviation of the parameterized subsurface temperature anomalies (contour intervals are every 0.25); (d)

Rms difference between the XBT and parameterized subsurface temperature anomalies over the period January 1993-May (contour intervals are every 0.1)

Figure 6: Time series of the observed (thick line) and simulated (thin line) sea surface temperature anomalies averaged in the Niño4, Niño3 and Niño1+2 boxes when the vertical mixing term (term 7) is set to zero. Statistical comparisons are presented in Table 1.

Figure 7: Spatial maps (130°E-80°W/15°S-15°N) of the standard deviation of observed sea surface temperature anomalies (contour intervals are every 0.2°C and values higher than 1°C are shaded), of the standard deviation of simulated sea surface temperature anomalies (experiment SST0; contour intervals are every 0.2°C and values higher than 1°C are shaded), of the correlation between the observed and simulated anomalies (contour intervals are every 0.1 from 0. to 0.8, and every 0.05 from 0.80 to 0.95; values higher than 0.7 are shaded) and of the rms difference between the two fields (contour intervals are every 0.2°C and values higher than 1°C are shaded).

Figure 8: Map of correlation between sea surface temperature and T/P sea level anomalies over the period January 1993-May 1998 (contour intervals are every 0.1).

Figure 9: Same as Figure 6, but for the experiment with a spatially constant vertical mixing coefficient.

Figure 10: Same as Figure 6, but for the experiment with a spatially variable vertical mixing coefficient.

Figure 11: Same as Figure 7, but for the experiment with a spatially variable vertical mixing coefficient.

Figure 12: Longitude-time plots of the 2°N-2°S averaged interannual anomalies of (a) sea level observed by TOPEX/POSEIDON (contours are every 5cm, negative values are shaded), (b) derived geostrophic zonal currents (contours are every 15cm/s, negative values are shaded), (c) observed SSTA (contours are every 0.5°C, negative values are shaded),

Figure 13: Same as Figure 12 but of (a) simulated sea level, (b) simulated zonal current anomalies, and (c) simulated sea surface temperature anomalies.

Figure 14: Time series of the simulated terms contributing to the sea surface temperature anomaly equation averaged in the Niño3 box .

Figure 15: Time series of the simulated terms contributing to the sea surface temperature anomaly equation averaged in the Niño4 box .

Figure 16: Longitude-time plots of the 2°N-2°S averaged interannual anomalies of: (a-c) same as in Figure 14a-c, but only the differences between the control run and the one with no eastern boundary reflection are plotted.

Figure 17: Same as Figure 14, but only the differences between the control run and the one with no eastern boundary reflection are plotted.

Figure 18: Same as Figure 16, but when the simulation is performed with no western boundary reflection.

Figure 19: Same as Figure 14, but only the differences between the control run and the one with no western boundary reflection are plotted.

	Niño1+2	Niño3	Niño4
	1.64	1.17	0.55
SST0	0.79	0.93	0.93
	0.90	1.14	0.60
	1.08	0.44	0.22
SST1	0.81	0.92	0.71
	1.80	1.40	0.58
	1.09	0.57	0.42
SSTR	0.81	0.93	0.94
	1.80	1.46	0.63
	1.09	0.57	0.23

Table 1: Evaluation of the simulated SSTA in the different boxes (Niño1+2, Niño3, Niño4) to observed indices for different experiments. In each column, the first value is the correlation, the second is the model standard variation, the third is the rms difference. In the first line, the standard deviation of observations are indicated for each Niño index.

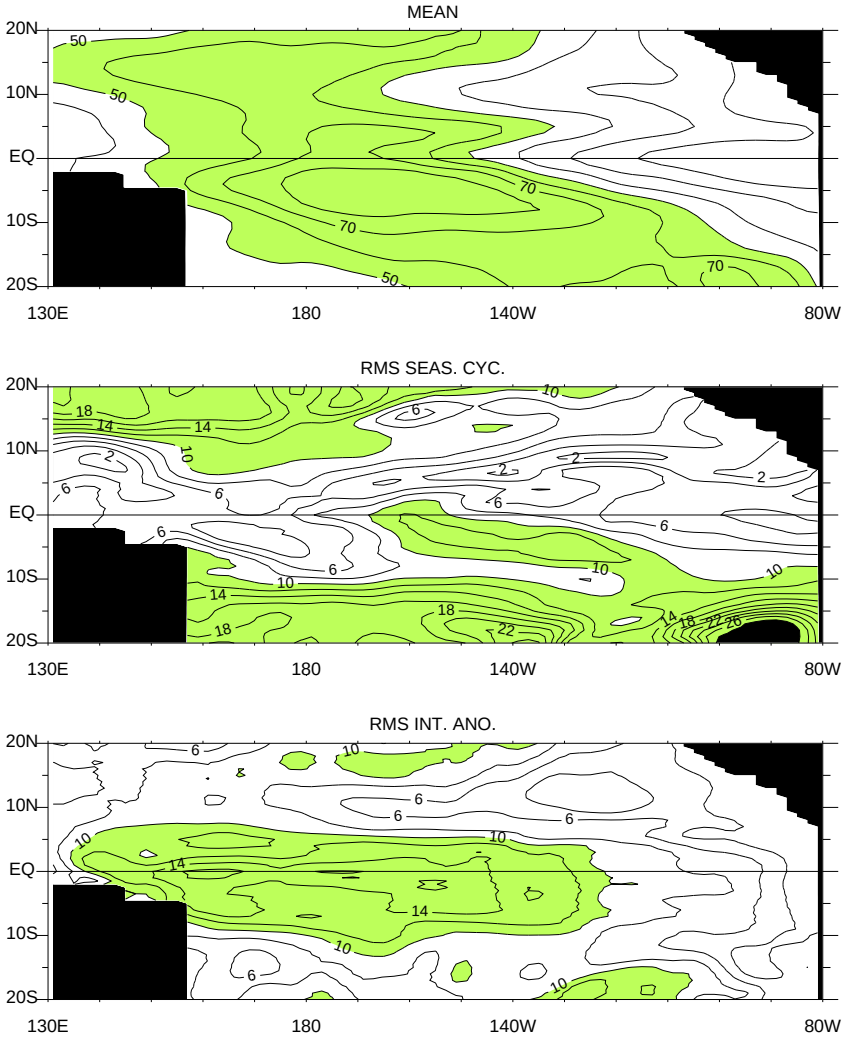
MEAN
20N
10N
EQ
10S
20S
130E
180
140W
80W
RMS SEAS. CYC.
RMS INT. ANO.

Figure 1:

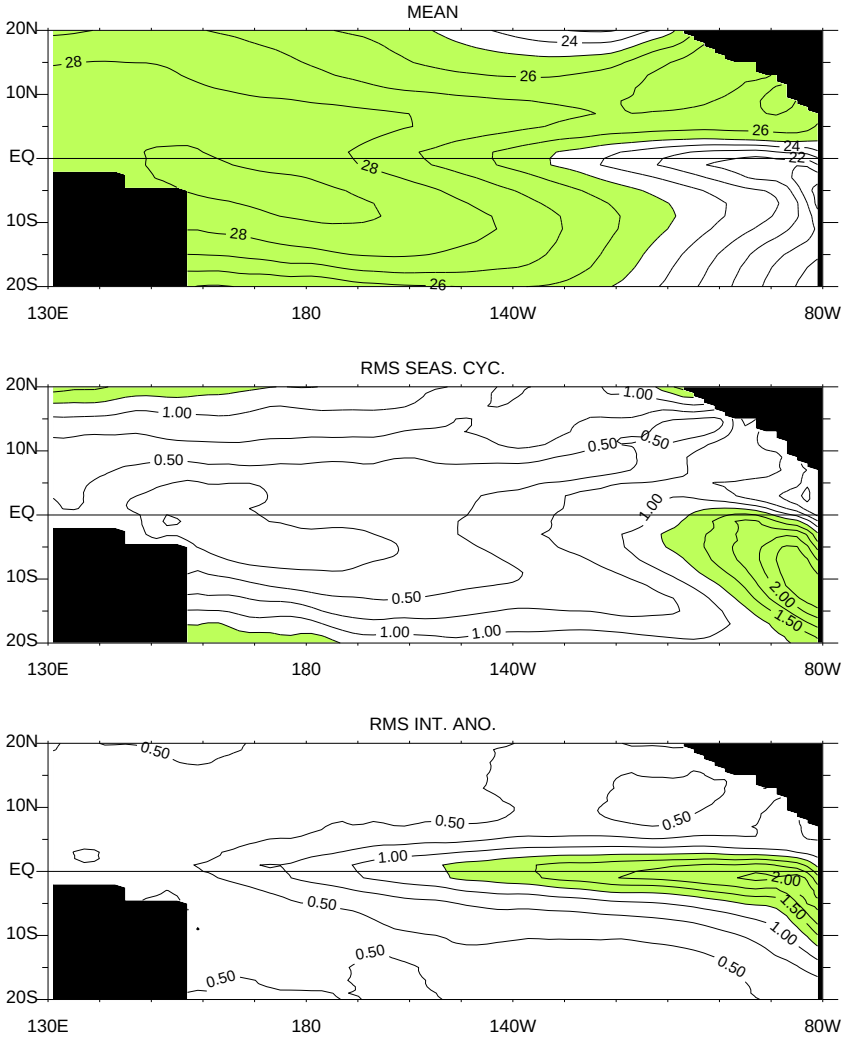
MEAN
20N
10N
EQ
10S
20S
130E
180
140W
80W
24
28
26
26
24
22
28
28
26
RMS SEAS. CYC.
1.00
1.00
0.50
0.50
0.50
1.00
2.00
1.50
0.50
1.00
1.00
RMS INT. ANO.
0.50
0.50
0.50
1.00
2.00
1.50
1.00
0.50
0.50
0.50

Figure 2:

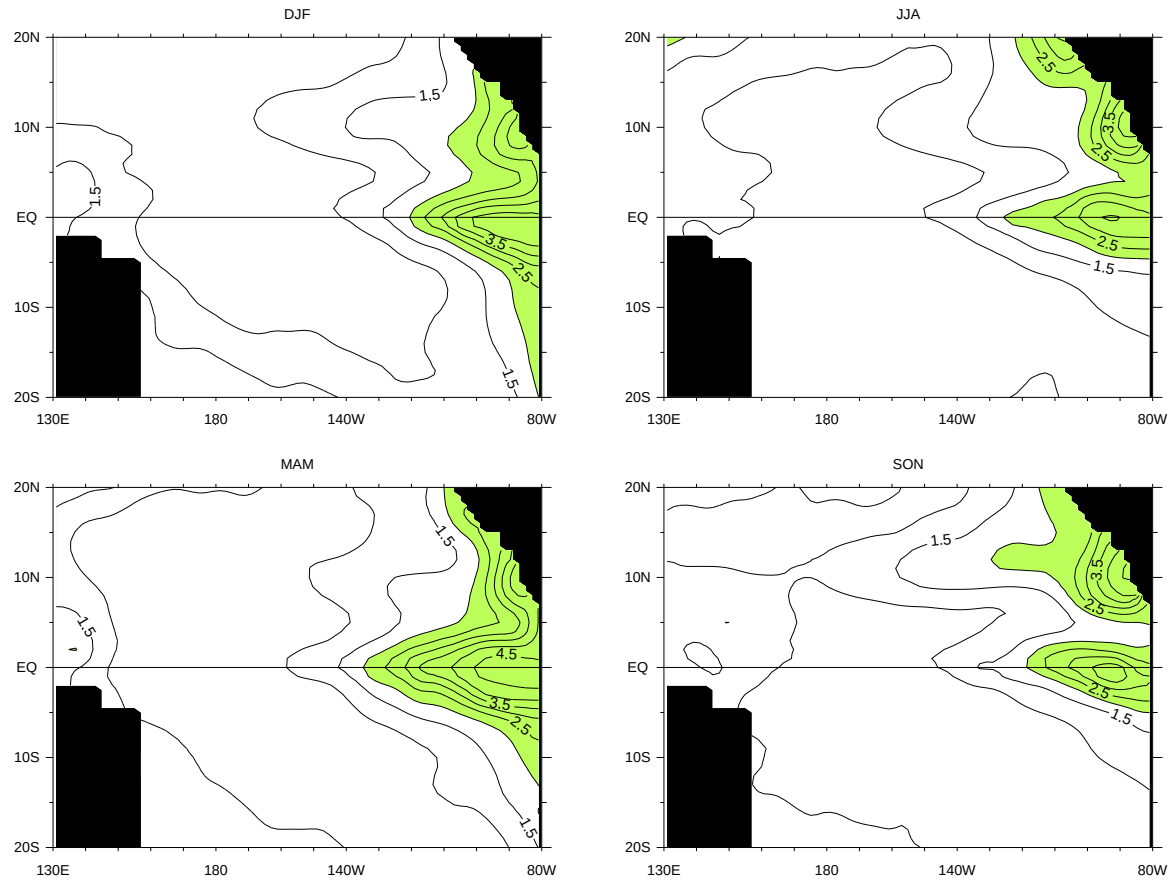

Figure 3:

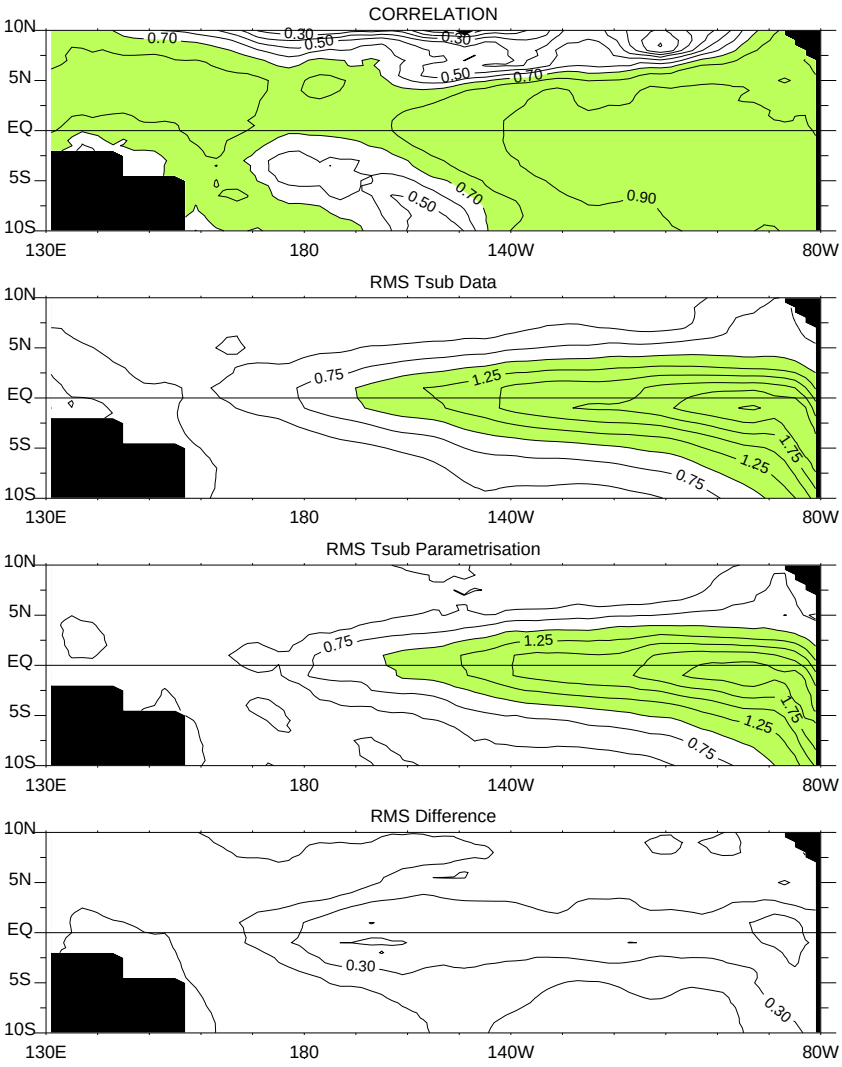
CORRELATION
10N
5N
EQ
5S
10S
130E
180
140W
80W
0.70
0.30
0.50
0.50
0.50
0.70
0.50
0.70
0.90
RMS Tsub Data
0.75
1.25
1.75
1.25
0.75
RMS Tsub Parametrisation
0.75
1.25
1.75
1.25
0.75
RMS Difference
0.30
0.30

Figure 4:

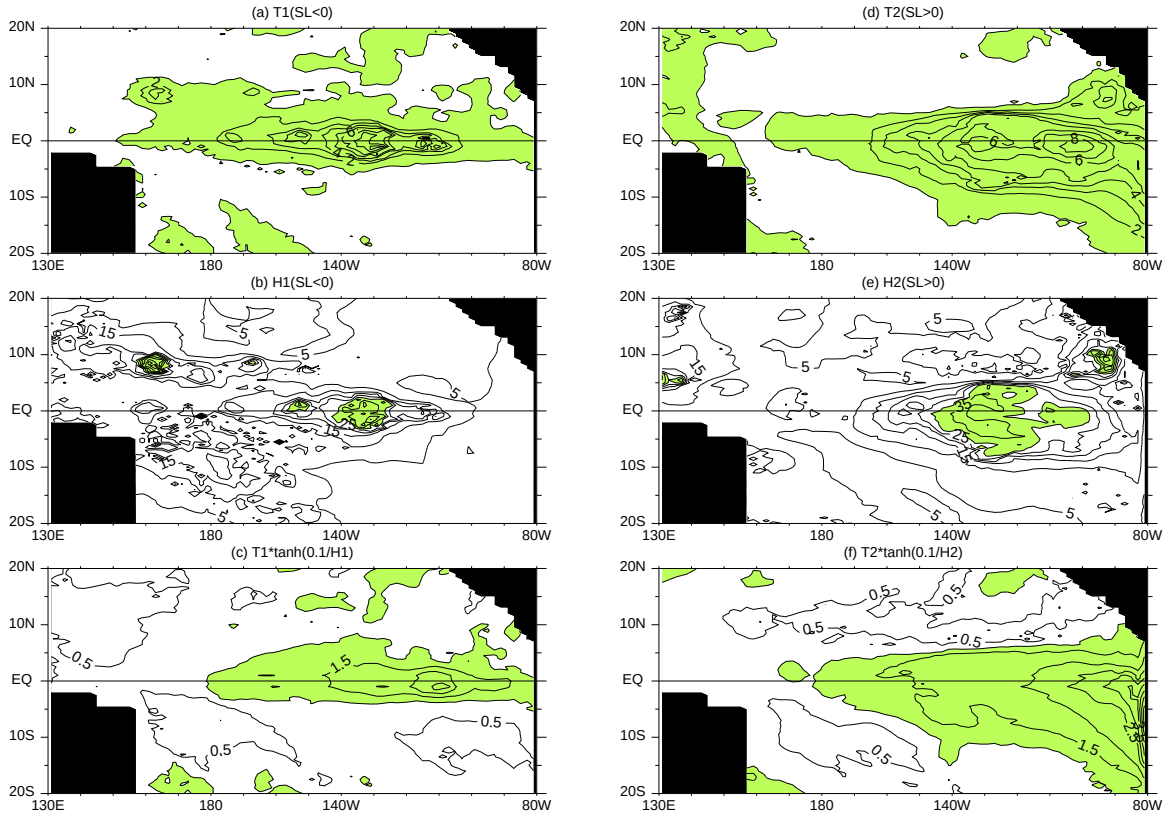
(a) T1(SL<0)
(d) T2(SL>0)
(b) H1(SL<0)
(e) H2(SL>0)
(c) T1*tanh(0.1/H1)
(f) T2*tanh(0.1/H2)
20N
10N
EQ
10S
20S
130E
180
140W
80W

Figure 5:

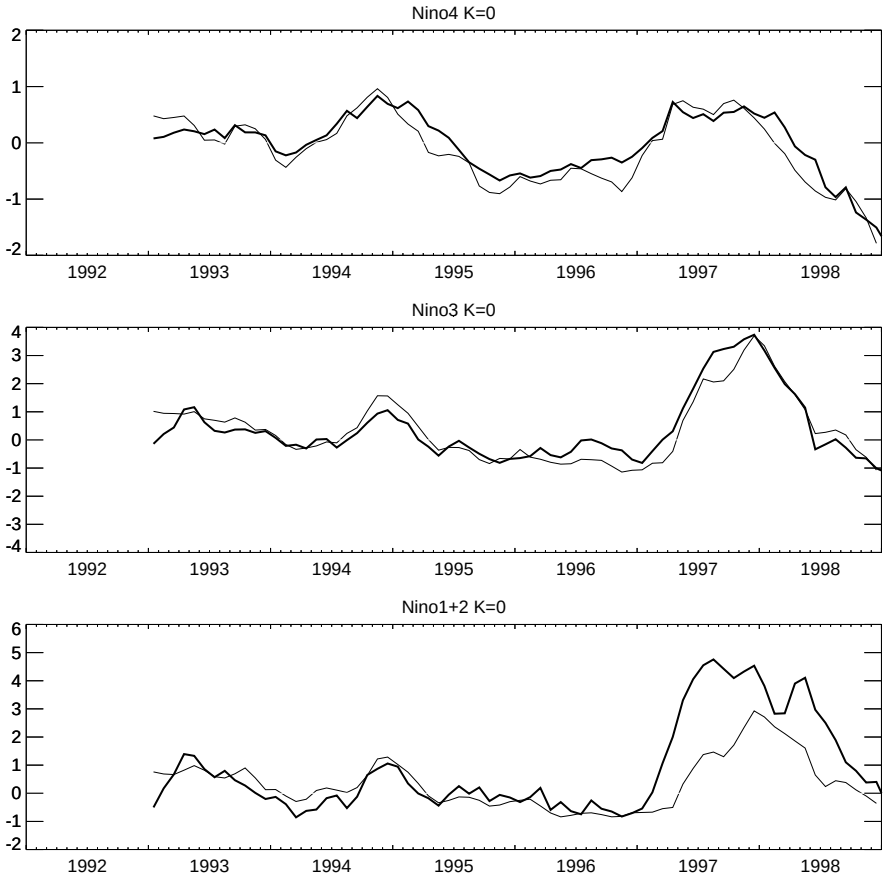
Nino4 K=0
2
1
0
-1
-2
1992
1993
1994
1995
1996
1997
1998
Nino3 K=0
4
3
2
1
0
-1
-2
-3
-4
1992
1993
1994
1995
1996
1997
1998
Nino1+2 K=0
6
5
4
3
2
1
0
-1
-2
1992
1993
1994
1995
1996
1997
1998

Figure 6:

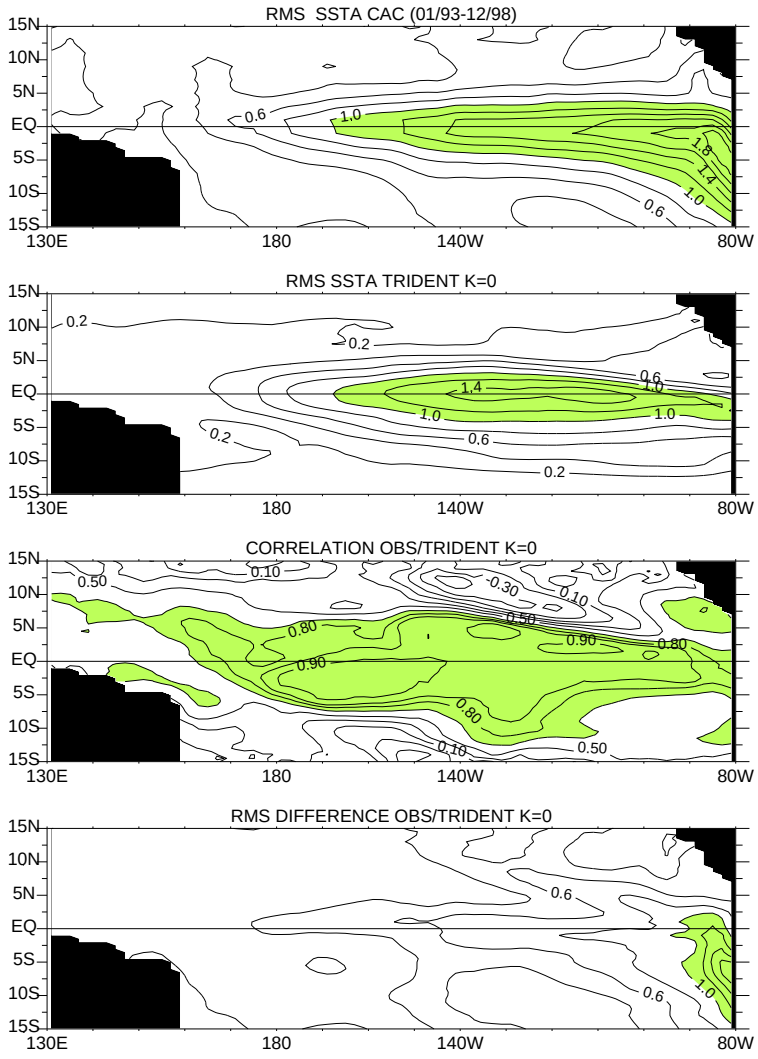
RMS SSTA CAC (01/93-12/98)
RMS SSTA TRIDENT K=0
CORRELATION OBS/TRIDENT K=0
RMS DIFFERENCE OBS/TRIDENT K=0
15N
10N
5N
EQ
5S
10S
15S
130E
180
140W
80W

Figure 7:

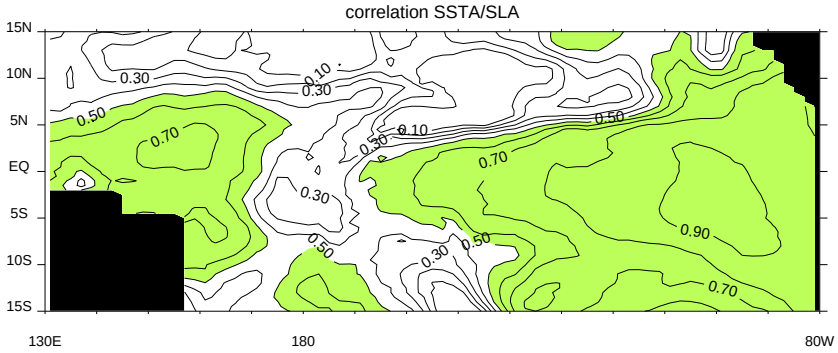
correlation SSTA/SLA
15N
10N
5N
EQ
5S
10S
15S
130E
180
80W
0.10
0.30
0.50
0.70
0.90

Figure 8:

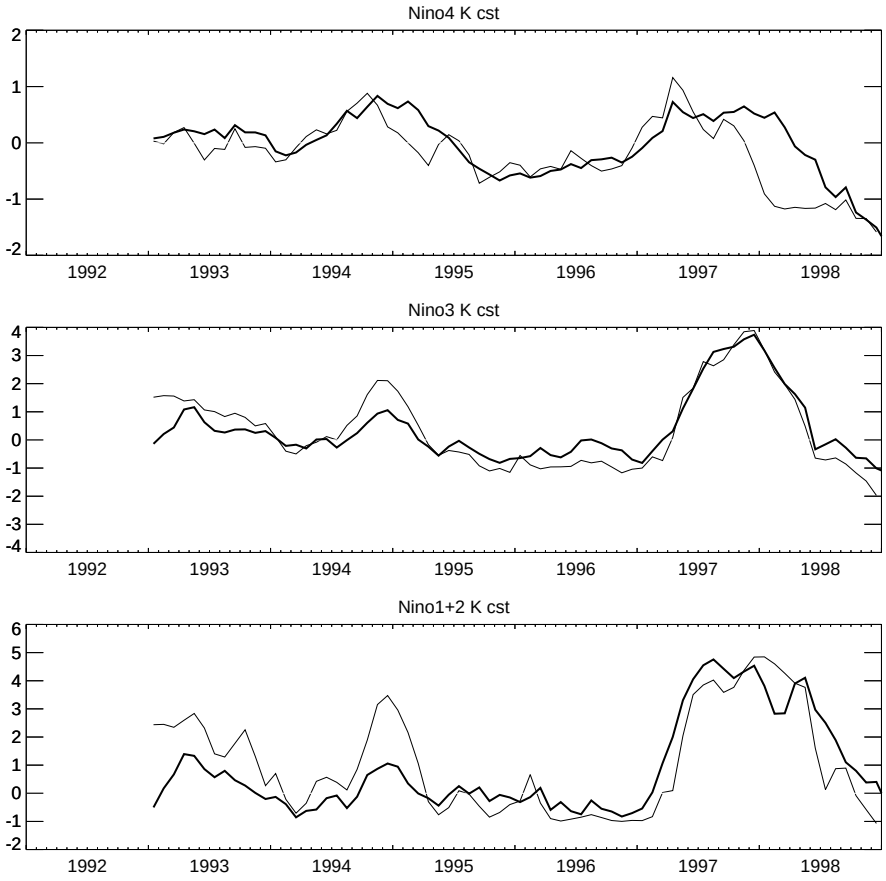
Nino4 K cst
2
1
0
-1
-2
1992
1993
1994
1995
1996
1997
1998
Nino3 K cst
4
3
2
1
0
-1
-2
-3
-4
1992
1993
1994
1995
1996
1997
1998
Nino1+2 K cst
6
5
4
3
2
1
0
-1
-2
1992
1993
1994
1995
1996
1997
1998

Figure 9:

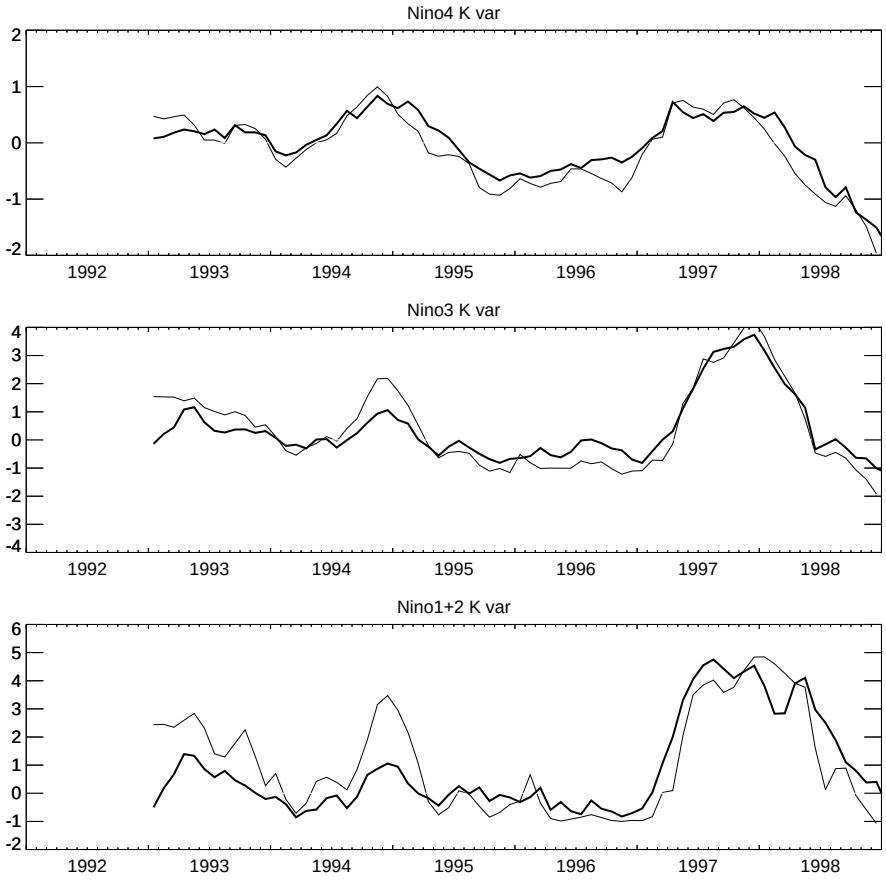
Nino4 K var
2
1
0
-1
-2
1992
1993
1994
1995
1996
1997
1998
Nino3 K var
4
3
2
1
0
-1
-2
-3
-4
1992
1993
1994
1995
1996
1997
1998
Nino1+2 K var
6
5
4
3
2
1
0
-1
-2
1992
1993
1994
1995
1996
1997
1998

Figure 10:

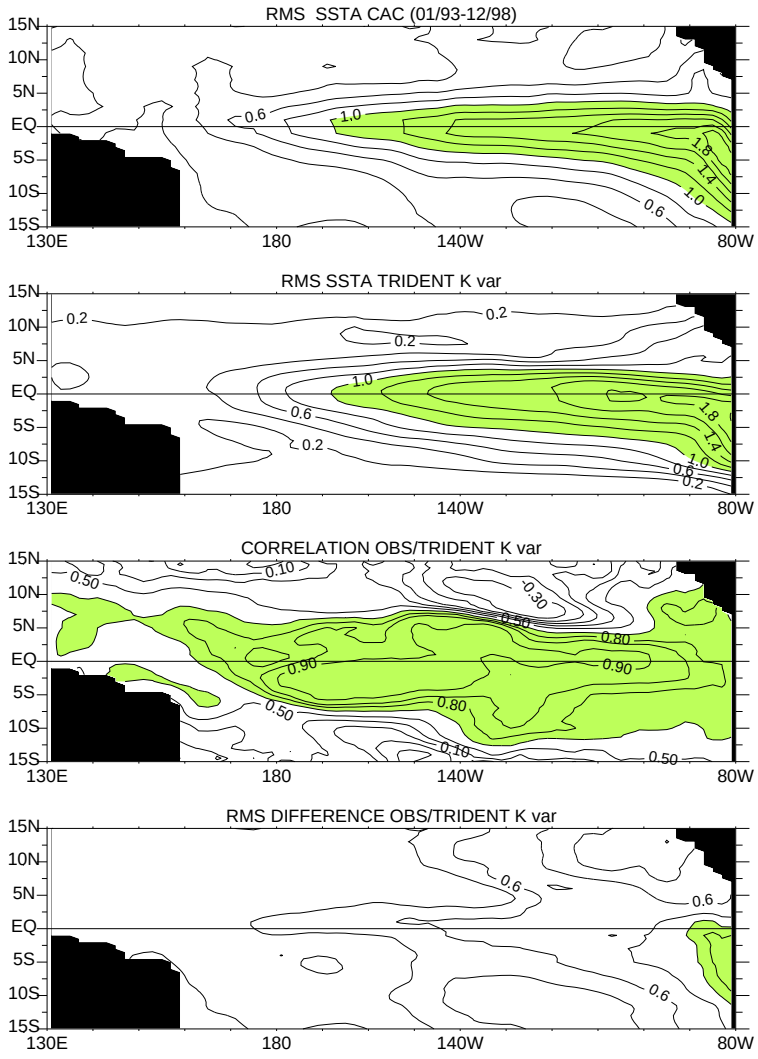
RMS SSTA CAC (01/93-12/98)
RMS SSTA TRIDENT K var
CORRELATION OBS/TRIDENT K var
RMS DIFFERENCE OBS/TRIDENT K var
15N
10N
5N
EQ
5S
10S
15S
130E
180
140W
80W

Figure 11:

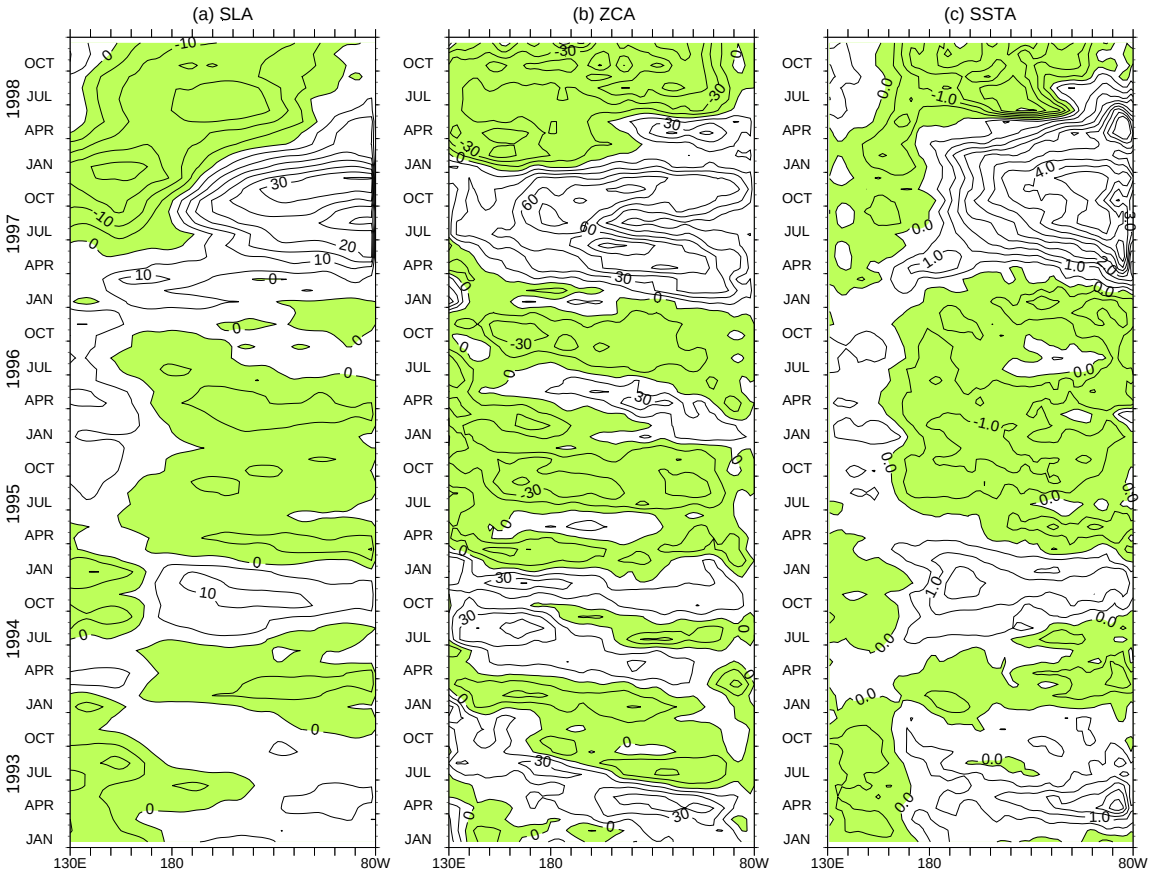
(a) SLA
(b) ZCA
(c) SSTA
1998
1997
1996
1995
1994
1993
OCT
JUL
APR
JAN
130E
180
80W

Figure 12:

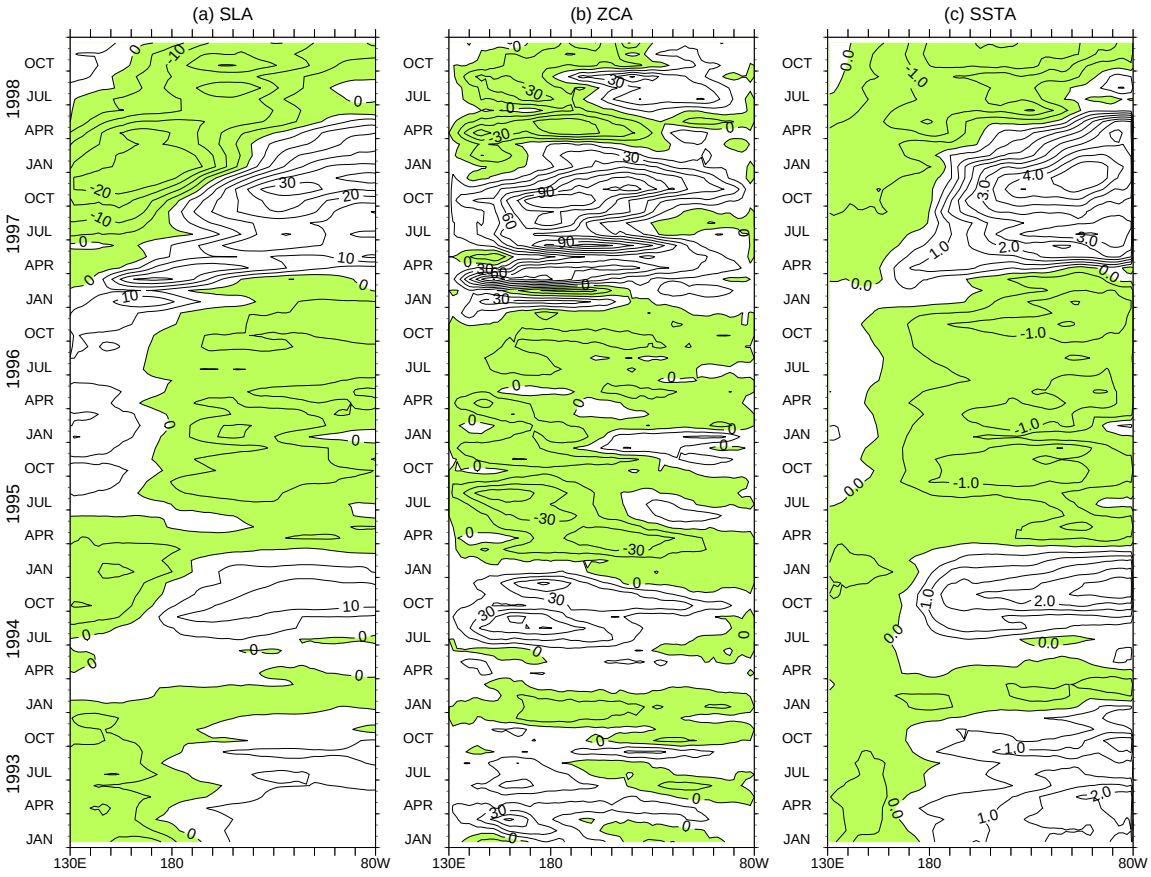
(a) SLA
(b) ZCA
(c) SSTA
1998
1997
1996
1995
1994
1993
OCT
JUL
APR
JAN
130E
180
80W

Figure 13:

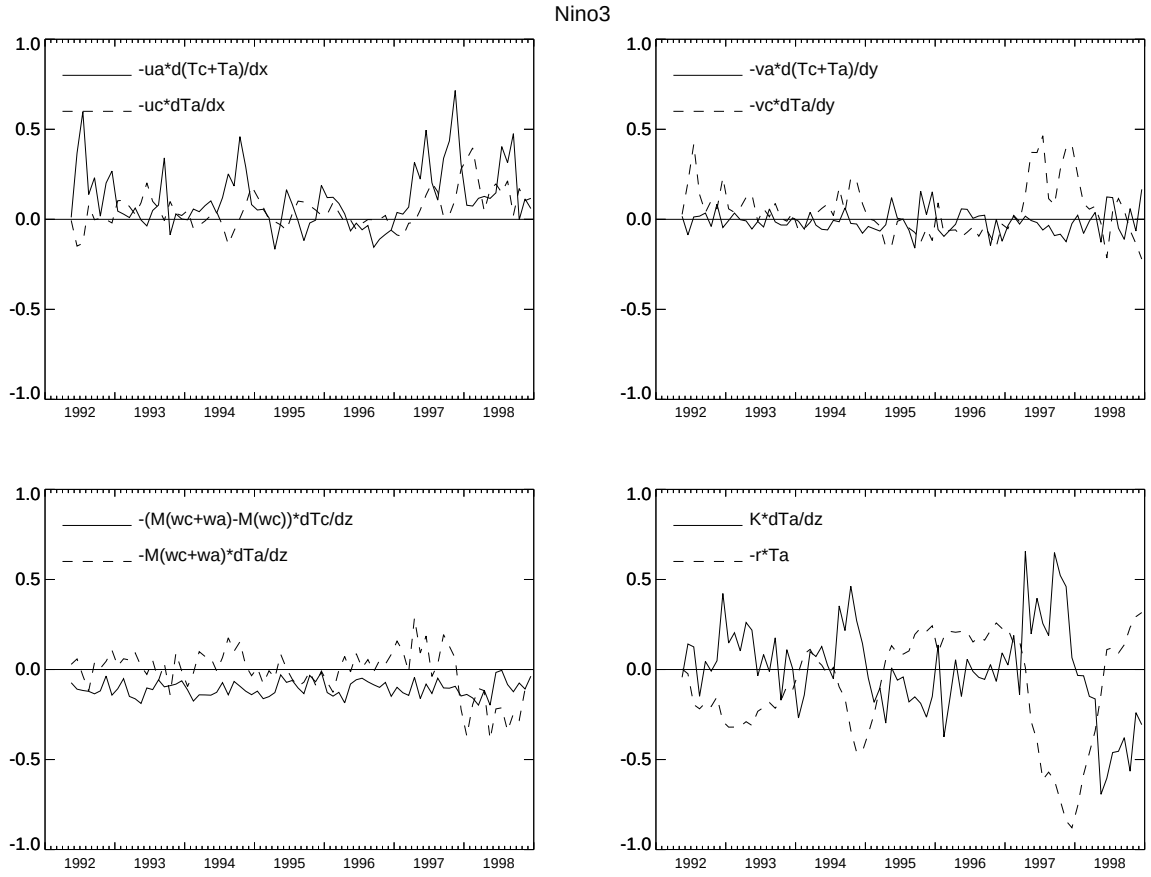
Nino3
-ua*d(Tc+Ta)/dx
-uc*dTa/dx
-va*d(Tc+Ta)/dy
-vc*dTa/dy
-(M(wc+wa)-M(wc))*dTc/dz
-M(wc+wa)*dTa/dz
K*dTa/dz
-r*Ta
1.0
0.5
0.0
-0.5
-1.0
1992
1993
1994
1995
1996
1997
1998

Figure 14:

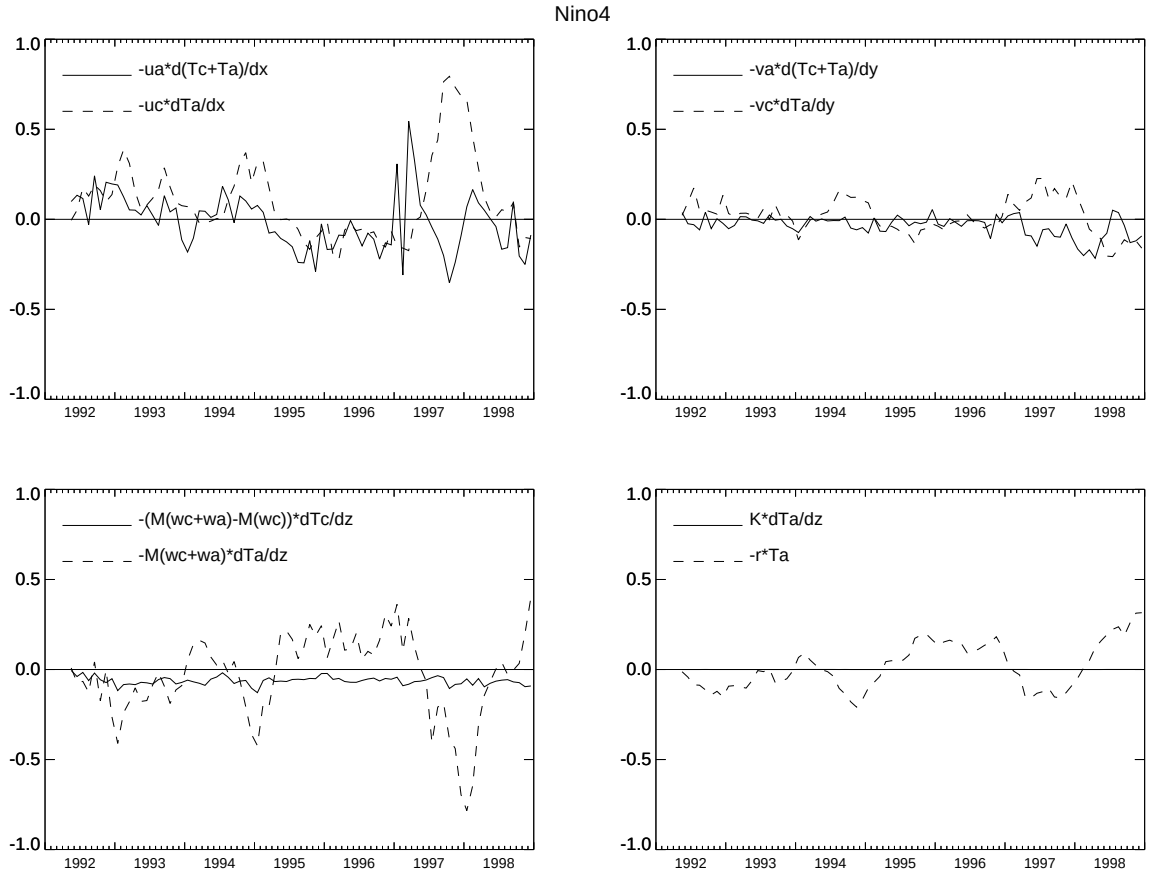
Nino4
-ua*d(Tc+Ta)/dx
-uc*dTa/dx
-va*d(Tc+Ta)/dy
-vc*dTa/dy
-(M(wc+wa)-M(wc))*dTc/dz
-M(wc+wa)*dTa/dz
K*dTa/dz
-r*Ta
1.0
0.5
0.0
-0.5
-1.0
1992
1993
1994
1995
1996
1997
1998

Figure 15:

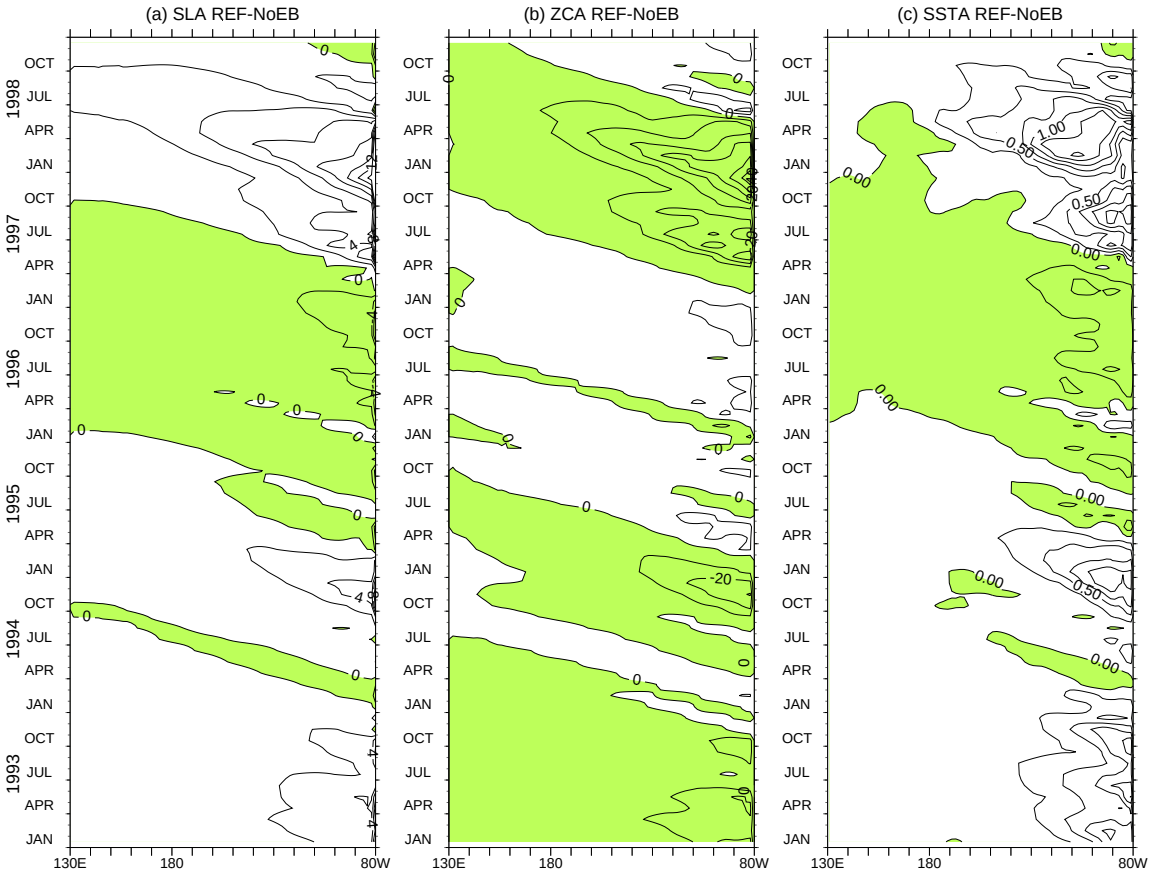
(a) SLA REF-NoEB
(b) ZCA REF-NoEB
(c) SSTA REF-NoEB
1998
1997
1996
1995
1994
1993
OCT
JUL
APR
JAN
130E
180
80W

Figure 16:

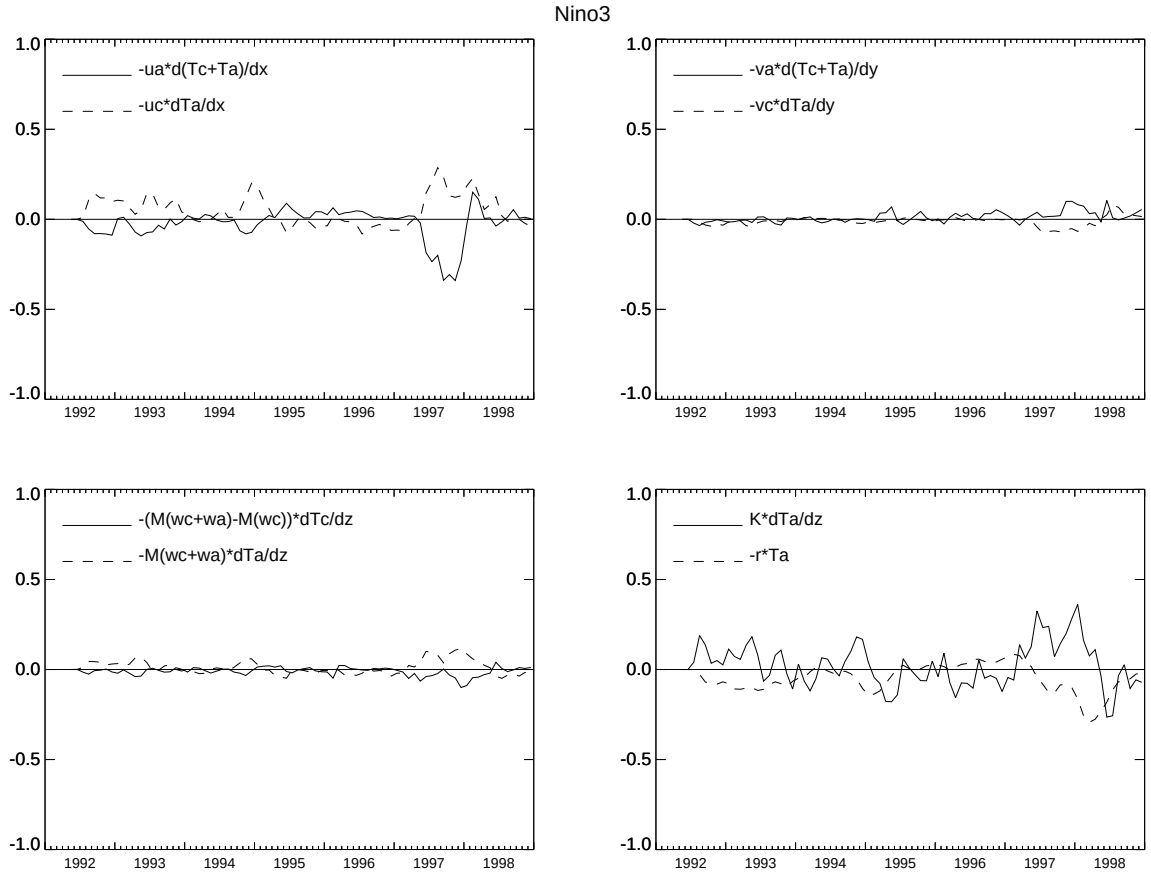
Nino3
-ua*d(Tc+Ta)/dx
-uc*dTa/dx
-va*d(Tc+Ta)/dy
-vc*dTa/dy
-(M(wc+wa)-M(wc))*dTc/dz
-M(wc+wa)*dTa/dz
K*dTa/dz
-r*Ta
1.0
0.5
0.0
-0.5
-1.0
1992
1993
1994
1995
1996
1997
1998

Figure 17:

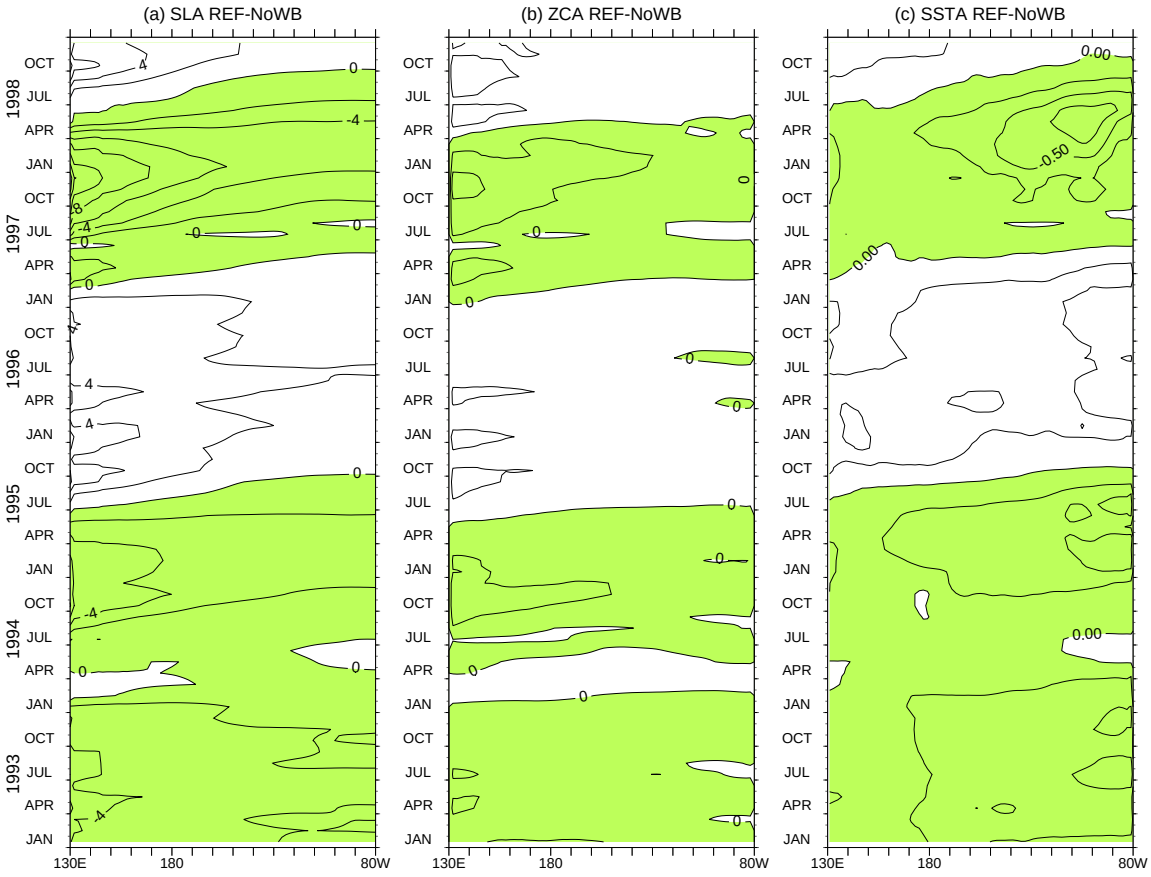
(a) SLA REF-NoWB
(b) ZCA REF-NoWB
(c) SSTA REF-NoWB
1998
1997
1996
1995
1994
1993
OCT
JUL
APR
JAN
130E
180
80W
0.00
-0.50

Figure 18:

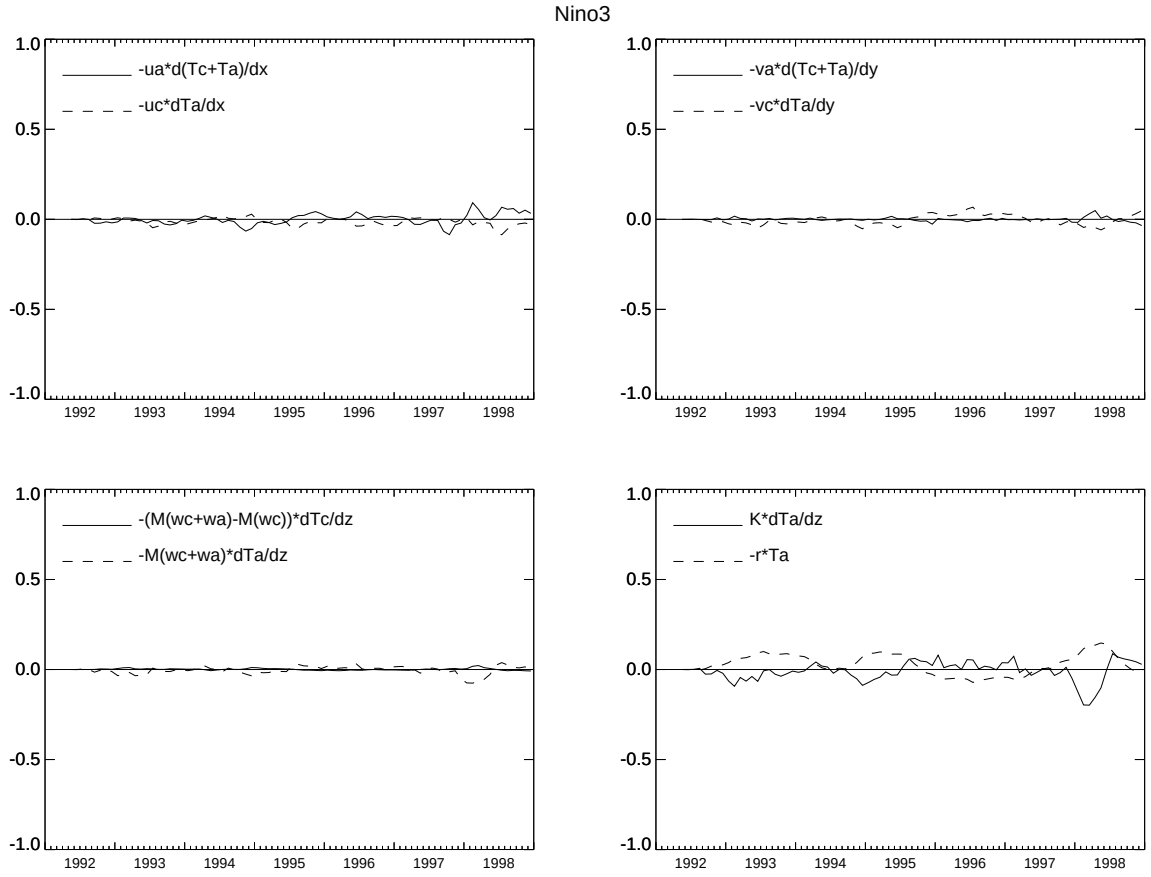
Nino3
-ua*d(Tc+Ta)/dx
-uc*dTa/dx
-va*d(Tc+Ta)/dy
-vc*dTa/dy
-(M(wc+wa)-M(wc))*dTc/dz
-M(wc+wa)*dTa/dz
K*dTa/dz
-r*Ta
1.0
0.5
0.0
-0.5
-1.0
1992
1993
1994
1995
1996
1997
1998

Figure 19:

Déjà paru :

4 : Mars 1998 Jérôme Vialard et Pascale Delecluse, *An OGCM Study for the TOGA Decade. Part I: Role of Salinity in the Physics of the Western Pacific Fresh Pool, Part II: Barrier layer formation and variability*

5 : Avril 1998 O. Aumont, J. C. Orr, P. Monfray, and G. Madec, *Nutrient trapping in the equatorial Pacific: The ocean circulation solution*

6 : Mai 1998 Emmanuelle Cohen-Solal and Hervé Le Treut, *Long term climate drift of a coupled surface ocean-atmosphere model : role of ocean heat transport and cloud radiative feedbacks*

7 : Juin 1998 Marina Lévy, Laurent Mémery and Gurvan Madec, *Combined Effects of Mesoscale Processes and Atmospheric High-Frequency Variability on the Spring Bloom in the MEDOC Area*

8 : Septembre 1998 Carine Laurent, Hervé Le Treut, Zhao-Xin Li, Laurent Fairhead and Jean-Louis Dufresne, *The influence of resolution in simulating interannual and inter-decadal variability in a coupled ocean-atmosphere GCM, with emphasis over the North Atlantic.*

9 : Octobre 1998 Francis Codron, Augustin Vintzileos and Robert Sadourny, *An Improved Interpolation Scheme between an Atmospheric Model and Underlying Surface Grids near Orography and Ocean Boundaries.*

10 : Novembre 1998 Z.X. Li and A.F. Carril, *Transient properties of atmospheric circulation in two reanalysis datasets.*

11 : Décembre 1998 Gurvan Madec, Pascale Delecluse, Maurice Imbard and Claire Lévy, *OPA8.1 ocean general circulation model reference manual.*

12 : Janvier 1999 Marc Guyon, Gurvan Madec, François-Xavier Roux, Christophe Herbaut, Maurice Imbard, and Philippe Fraunie*Domain Decomposition Method as a Nutshell for Massively Parallel Ocean Modelling with the OPA Model .*

13 : Février 1999 Eric Guilyardi, Gurvan Madec, and Laurent Terray *he Role of Lateral Ocean Physics in the Upper Ocean Thermal Balance of a Coupled Ocean-Atmosphere GCM*

14 : Mars 1999 D. Hauglustaine *Impact of Biomass Burning and Lightning Emissions on the Distribution of Tropospheric Ozone and its Precursors in the Tropics*

15 : Décembre 1999 L. Menut, R. Vautard, C. Honnoré, and M. Beekmann *Sensitivity of Photochemical Pollution using the Adjoint of a Simplified Chemistry-Transport Model*

16 : Janvier 2000 J.-Ph. Boulanger *The Trident Pacific model. Part 1: The oceanic dynamical model and observations during the TOPEX/POSEIDON period*

17 : Janvier 2000 J.-Ph. Boulanger and Christophe Menkes *The Trident Pacific model Part 2: The thermodynamical model and the role of long equatorial wave reflection during the TOPEX/POSEIDON period*

Plus de détails sont disponibles sur Internet :
http://www.ipsl.jussieu.fr/modelisation/liste-notes.html.